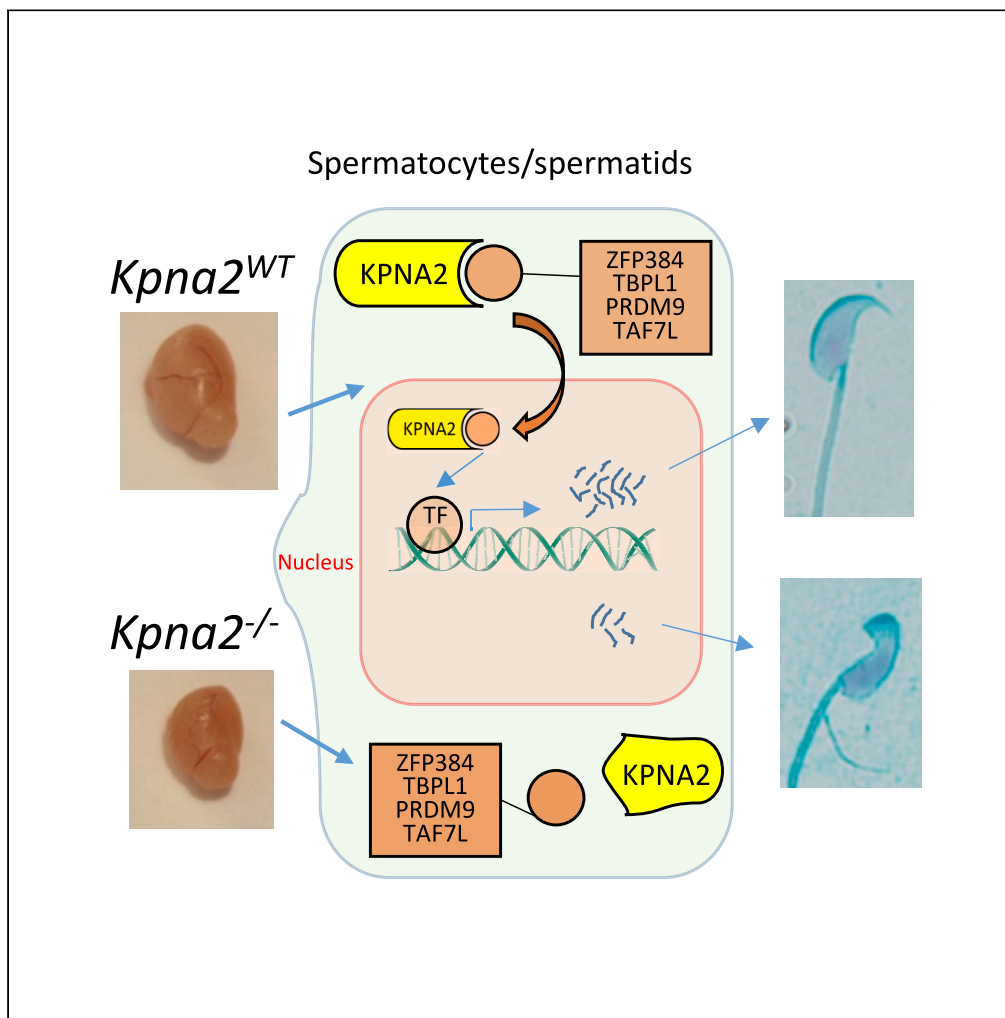


Article

Loss of the importin *Kpna2* causes infertility in male mice by disrupting the translocation of testis-specific transcription factors



Paula Navarrete-López, María Maroto, Eva Pericuesta, Raúl Fernández-González, Marta Lombó, Priscila Ramos-Ibeas, Alfonso Gutiérrez-Adán

agutierr@inia.csic.es

Highlights

Kpna2 is essential to produce functional spermatozoa in mice testis

Loss of *Kpna2* alters the transcriptional program required for spermatogenesis

Testis transcription factors were enriched around the promoters of downregulated genes

KPNA2 is proposed to control the nuclear import of factors specific to spermatogenesis

Navarrete-López et al.,
iScience 26, 107134
July 21, 2023 © 2023 The Author(s).
<https://doi.org/10.1016/j.isci.2023.107134>



Article

Loss of the importin *Kpna2* causes infertility in male mice by disrupting the translocation of testis-specific transcription factors

Paula Navarrete-López,¹ María Maroto,¹ Eva Pericuesta,¹ Raúl Fernández-González,¹ Marta Lombó,¹ Priscila Ramos-Ibeas,¹ and Alfonso Gutiérrez-Adán^{1,2,*}

SUMMARY

Karyopherins mediate the movement between the nucleus and cytoplasm of specific proteins in diverse cellular processes. Through a loss-of-function approach, we here examine the role of Karyopherin Subunit Alpha 2 (*Kpna2*) in spermatogenesis. Knockout male mice exhibited reduced body size and sperm motility, increased sperm abnormalities, and led to the dysregulation of testis gene expression and ultimately to infertility. Impaired mRNA expression mainly affected clusters of genes expressed in spermatids and spermatocytes. Downregulated genes included a set of genes that participate in cell adhesion and extracellular matrix (ECM) organization. We detected both the enrichment of some transcription factors that bind to regions around transcription start sites of downregulated genes and the impaired transport of specific factors to the nucleus of spermatid cells. We propose that *Kpna2* is essential in the seminiferous tubules for promoting the translocation of testis-specific transcription factors that control the expression of genes related to ECM organization.

INTRODUCTION

The molecular events controlled by the distribution of proteins in the nuclear and cytoplasmic compartments are essential during spermatogenesis. The nucleocytoplasmic transport machinery tightly coordinates gene expression patterns by mediating transport into and out of the nucleus of transcription factors and other proteins involved in functions such as mRNA processing, mitosis/meiosis, and chromatin remodeling, thereby controlling different cell processes including cell proliferation and differentiation, pluripotency maintenance, organism development, DNA repair, and cell migration.^{1–6} The carrier molecules that enable the transport of cargo proteins through the nuclear pore complex embedded in the nuclear envelope are the karyopherin (KPN) family of proteins, consisting of more than twenty proteins categorized into two groups, α and β . Karyopherin α s are importins often termed importin α s, while karyopherin β s have roles in nuclear import and export. The different α importins have distinct binding specificities, expression patterns, and subcellular localizations in different cell types, indicating specialized cell roles. Moreover, there is evidence that α importins contribute to functions other than nucleocytoplasmic transport, including transcriptional regulation,^{7,8} spindle assembly,⁹ or nuclear envelope formation.¹⁰ Moreover, importin α members are known to build up in the nucleus under stress conditions such as heat shock and oxidative stress, wherein they bind to a DNase-sensitive nuclear component.⁷ Further, the bifunctionality of the importin 2α N-terminal region for nuclear transport and chromatin association has been described⁸ and several examples of protein anchoring in the cytoplasm by importins have been reported.¹¹

The dysregulation of certain importins has been associated with a variety of disorders including multiple cancer types¹² as well as neurodegenerative diseases,¹³ along with infertility.^{14,15} Several studies have described the role of karyopherin alpha proteins (KPNAs) in male and female gametogenesis.^{16–19} Given the complex nature of the multi-stage process of male germ cell differentiation, the controlled entry of factors regulating transcriptional activity is essential for the accurate tuning of regulatory mechanisms. Knockouts (KOs) for several importin α s in mice displayed distinct phenotypes.^{15,20,21} Hence, female *Kpna1*, *Kpna6*, and *Kpna8* KOs and male *Kpna4* and *Kpna6* KOs show impaired fertility (discussed below), while no phenotype of *Kpna3* KOs has been identified.^{14,22,23} No mouse line lacking *Kpna2* has been reported. The absence of importin *Kpna4* in the testis led to the identification of subfertility traits in mice (reduced

¹Department of Animal Reproduction, INIA-CSIC, 28040 Madrid, Spain

²Lead contact

*Correspondence: agutierr@inia.csic.es

<https://doi.org/10.1016/j.isci.2023.107134>



quality and motility of sperm and reduced offspring size).¹⁴ KPNA2 is known to be the most expressed importin in embryonic mouse testis (from sex determination to shortly after birth) as well as in adult testis throughout spermatogenesis,²⁴ suggesting a central role as a key mediator of nucleocytoplasmic transport in the testis and/or other unexplored functions. This importin shows a dynamic cell type-specific pattern throughout the process of spermatogenesis in the seminiferous tubules, where it is localized in the nucleus of pachytene spermatocytes, the cytoplasm of round spermatids, and the cytoplasm and nucleus of elongating spermatids.²⁵ Moreover, several binding partners of KPNA2 that exert their function in the nucleus have been identified in testis.²⁵ According to the testicular expression pattern of *Kpna2* and its dynamic subcellular localization during the differentiation process and cargoes identified in the testis, it has been hypothesized that KPNA2 may play a critical role throughout spermatogenesis.

To understand the role of KPNA2 in the testis, we designed a *Kpna2*-KO mouse model to provide insight into the regulatory networks controlled by *Kpna2* in the process of sperm production. Based on the phenotypic characterization and transcriptomic analysis of these mice, we found that *Kpna2* controls directly or indirectly the expression of specific clusters of genes during spermatogenesis.

RESULTS

Kpna2 is essential for male fertility

To determine the role of *Kpna2* during mammalian spermatogenesis, we used CRISPR-Cas9 technology to produce *Kpna2*-KO mice with exon 2 deletion (Figure 1A). From the transgenic mice generated, two lines were selected with deletions of 4 and 8 nt (*Kpna2*^{-/-} lines 4 and 7, respectively) that gave rise to a predicted frameshift and early chain termination due to a premature stop codon generating proteins of 30 aa and 31 aa instead of the wild-type (WT) protein consisting of 529 aa (Figures 1B and 1C). Both alleles were transmitted to the next generation after breeding. As the two lines showed similar phenotypes, the following phenotyping results refer to *Kpna2*^{-/-} line 4. Male and female *Kpna2* heterozygotes were normal and fertile, and we generated homozygous KOs by inter-crossing heterozygotes. Quantitative analysis of *Kpna2* expression in the homozygous testis revealed a dramatic reduction in the signal when compared to controls (Figure 1D). In western blot and immunofluorescence analyses, KPNA2 was found to be absent in the testes of *Kpna2*^{-/-} mice (Figures 1E, 1G, and S1). Male and female homozygous KO mice were also smaller than WT or heterozygous mice (Figure S2).

We then examined the outcomes of mating KO mice in terms of litter sizes and offspring genotypes. Crosses between males and females heterozygous *Kpna2*^{+/-} mice produced an average litter size of 5.8 (total 35 matings), smaller than the WT litter average of 7.4 ($p < 0.01$, t-student). Genotypes of offspring from mating *Kpna2*^{+/-} females and males did not display a Mendelian ratio (1.34:2.44:0.22), and there were no differences in the sex ratios of the offspring (Figure 1F), indicating the loss of KO embryos during the preimplantation or fetal stage. When *Kpna2*^{-/-} male mice were mated with WT females, these animals proved infertile (20 males crossed with 2 females each were analyzed). No differences were detected in apoptotic cell rates recorded for the testis of *Kpna2*^{-/-} male and WT mice (4.2 ± 4 vs. 3.9 ± 7 , respectively). To try to understand the reason for the observed infertility, we calculated testis/body weight ratios and examined the testis, but no differences emerged in testis weight, sperm concentration, or sperm viability (Figures 2A, 2B, and S3A). Moreover, we found no differences in the appearance of testis cross-sections (Figure S1). Differences between *Kpna2*^{-/-} and WT mice were detected in sperm abnormality percentages, which emerged as significant for head, neck, and midpiece defects ($p < 0.01$, ANOVA) (Figures 2I and 2J), suggesting a role of KPNA2 in maintaining normal sperm head morphology. In addition, *Kpna2*^{-/-} sperm showed lower total and progressive motility than WT sperm (Figures 2C and 2D). In our computer-assisted sperm analysis (CASA) of sperm motility, we observed reduced kinetic parameters VSL, VAP, LIN, and STR in the *Kpna2*^{-/-} sperm (Figures 2E–2H) but no differences in the remaining CASA parameters (Figures S3C–S3F), indicating a reduction in linearity and straightness of spermatozoa, along with their reduced progressive motility (Videos S1A and S1B).

To analyze the DNA integrity of the *Kpna2*^{-/-} sperm, we examined fertilization rates in response to intracytoplasmic sperm injection (ICSI). Fertilization and cleavage rates were similar for *Kpna2*^{-/-} and WT sperm (78% vs. 75% cleavage embryos and 47% vs. 51% blastocysts using *Kpna2*^{-/-} or WT sperm, respectively, $n = 4$ experiments). These data rule out DNA alterations or embryonic losses during preimplantation development as the cause of *Kpna2*^{-/-} infertility, suggesting that, *in vivo*, the *Kpna2*^{-/-} spermatozoon is unable to fertilize oocytes.

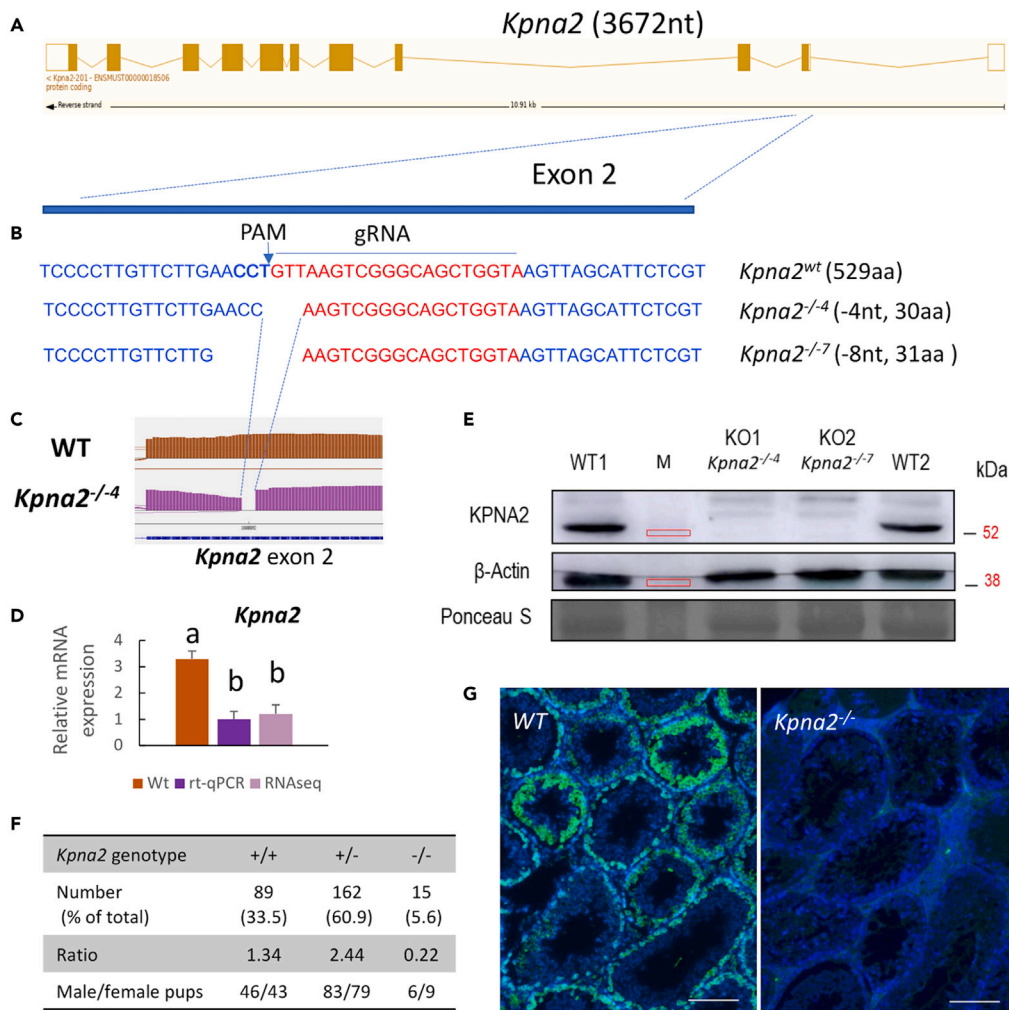


Figure 1. Diagrams of *Kpna2*-KO lines produced by CRISPR-Cas9 and their mRNA and protein expression

(A) The *Kpna2* gene consists of 11 exons (vertical lines).

(B) Nucleotide deletions produced by CRISPR-Cas9 in exon 2 of the transgenic mouse lines *Kpna2*^{-/-4} and *Kpna2*^{-/-7}. Superscript numbers indicate nucleotides deleted and amino acids encoded by the WT and mutant proteins. Red letters indicate the guide RNA (gRNA). PAM sequences are indicated in bold blue.

(C) RNA-seq coverage plot of the *Kpna2* gene representing the WT data (brown) and the *Kpna2*^{-/-4} data (purple). The upper panel provides a zoom of *Kpna2*'s exon 2, showing the coverage and deletion of the mutant. The lower panel shows the size of exon 2 in *Kpna2*^{-/-4}.

(D) Relative mRNA expression of *Kpna2* in the testis of WT and *Kpna2*^{-/-4} mice measured by RT-qPCR and RNA-seq. Data represent the mean ± SEM.

(E) Western blot analysis of KPNA2 protein expression in the testes of 2 WT and 2 *Kpna2*^{-/-} mice, using ACTB as a loading control and Ponceau S as a staining control of total protein. The positions of molecular mass markers are indicated in the M lane.

(F) Litter sizes and offspring genotypes of crosses between *Kpna2*^{+/-} (heterozygous) mice.

(G) Representative images of cross-sections of seminiferous tubules of WT and *Kpna2*^{-/-} mice stained with nuclear dye Hoechst (blue) and KPNA2 visualized with FITC-mouse antigoat antibody (green). Scale bar 200 μm.

Kpna2 expression patterns in mouse testis

In adult testes, KPNA2 was not detected in Sertoli cells but was abundant in germ cells, increasing from a moderate signal in spermatogonia and primary spermatocytes to a peak in pachytene spermatocytes and early round spermatids and becoming low in elongating spermatids to absent in condensing spermatids (Figure 3). KPNA2 is mainly located in the cytoplasm of testicular cells except in spermatogonia, pachytene spermatocytes, and early round spermatids, where the protein signal is nuclear and cytoplasmic (Figures 3

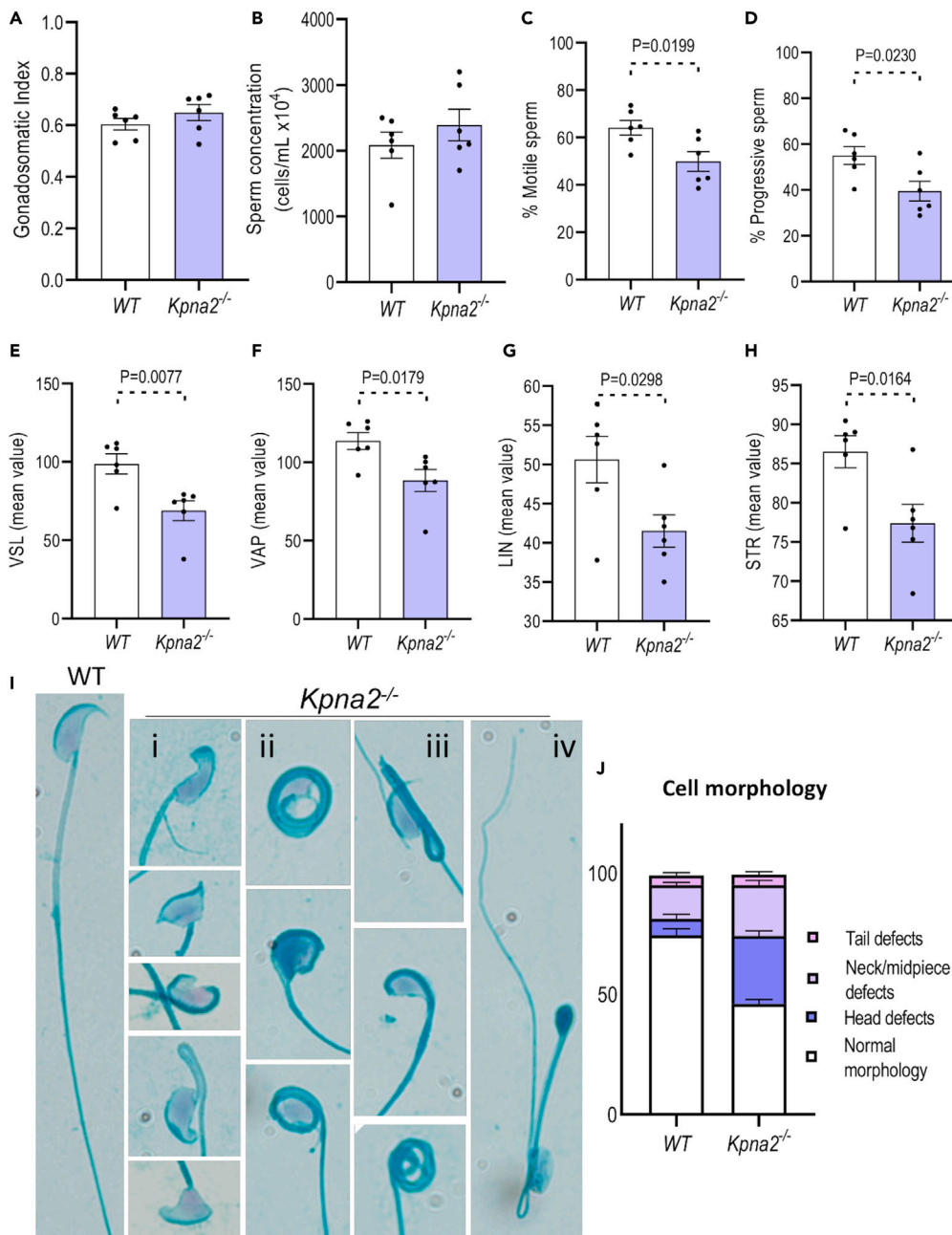


Figure 2. Sperm characteristics in wild type and *Kpna2*^{-/-} mice. Sperm was obtained from cauda epididymis and analyzed as described in Materials and Methods

(A and B) No differences were found in the gonadosomatic index or (B) sperm concentrations.

(C–H) Significant differences were observed between WT and *Kpna2*^{-/-} mice in sperm motility (n = 6 WT, and 7 *Kpna2*^{-/-} mice) and in some sperm motility parameters of spermatozoa (VSL, VAP, LIN, and STR).

(I) Examples of normal WT and abnormal (i–iv) sperm isolated from the cauda epididymis of *Kpna2*^{-/-} mice (stained with Spermac stain kit and observed under a standard bright-field microscope). Around 50% of sperm show some type of abnormality including neck and midpiece defects (ii–iii), head defects (i–iv), and tail defects (iii–iv). Significant differences were found in sperm morphology (n = 6 WT, and 6 *Kpna2*^{-/-} mice).

(J) Proportion of morphology categories of WT and *Kpna2*^{-/-} sperm. Data represent the mean ± SEM (one-way ANOVA, Tukey's test).

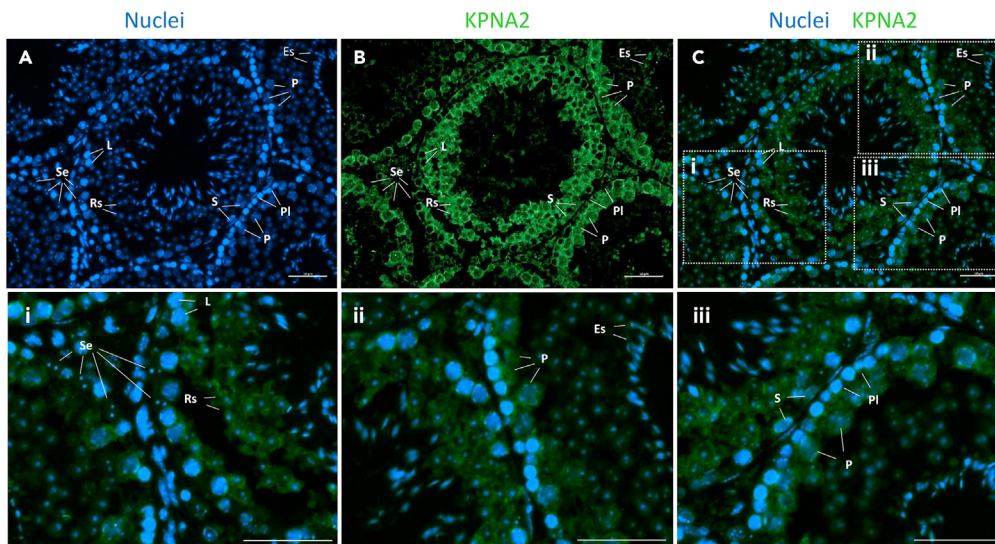


Figure 3. Immunolocalization of KPNA2 during spermatogenesis in mice testicles

Representative images of cross-sections of seminiferous tubules (A) stained with nuclear dye Hoechst (blue), (B) KPNA2 visualized with FITC conjugated secondary antibody (green), and (C) merged. Se, Sertoli cells; S, spermatogonia; PI, preleptotene spermatocytes; L, leptotene spermatocytes; P, pachytene spermatocytes; Rs, round spermatids; Es, elongated spermatids. Scale bar: 50 μ m.

and S1). In Figure 3, we can see the cytoplasmic signal in preleptotene and leptotene spermatocytes, while in spermatogonia, pachytene spermatocytes, and round spermatids, both the cytoplasmic and nuclear signals are visible. The most intense signals manifested in pachytene spermatocytes and early spermatids, and a non-specific signal was found in Leydig cells (Figure S1).

Gene expression in *Kpna2*^{-/-} mice

To decipher the molecular mechanisms underlying infertility, mRNA was analyzed in 4 wild types and 4 *Kpna2*^{-/-} testis samples. The processing of RNA sequencing (RNA-seq) data yielded an average of \sim 34 million paired-end reads across samples solely aligned toward the reference genome. Next, the read quantification led to the detection of \sim 23,800 RNAs among samples, considering a gene as expressed with raw counts above 10 (Table S2). The first principal component separated *Kpna2*^{-/-} from WT samples, and the hierarchical clustering of samples indicated a similar within-conditions gene expression pattern (Figures S4A and S4B).

We observed clear dysregulation at the transcriptomic level in *Kpna2*-KO testes where 3,891 genes were differentially expressed, as detailed in Table S2. The number of upregulated genes was 2,007, greater than the number of downregulated genes which was 1,884 (Table S2). Conversely, when increasing the fold change threshold, we found that downregulated genes outnumbered upregulated ones, as illustrated in the volcano plot (Figure 4A). Moreover, there were 103 differentially expressed genes (DEGs) showing considerably high fold changes (Figure 4B). We should highlight *Klrb1* gene as the most upregulated, showing no expression in WT testis with a considerable increase in mutants. *Klrb1* belongs to the c-type lectin-like natural killer receptors encoded by genes in the genomic region natural killer gene complex (NKC). Interestingly, among the top genes displaying the greater differences, we also found the NKC receptors *Klrb1c*, *Klra9*, and *Klra8* (Figure 4B), also upregulated, and the *Clec2e* and *Clec2h* genes (C-type lectin domain family members), which were downregulated, code for ligands of these receptors, and are located in the same genomic region. It seems that *Kpna2* may be inhibiting somehow the expression of *Klrb1* and other c-type lectin-like receptors, so the absence of *Kpna2* could have triggered their expression. Both *Kpna2* and *Klrb1* are known to play opposite roles in cancer. Hence, while the excessive expression of *Kpna2* is known to promote the proliferation and migration of (lung) cancer cells,²⁶ *Klrb1* is downregulated in most tumors and its expression is associated with a more favorable outcome of non-small-cell lung cancer.

In this context, we searched for gene clusters using Cluster Locator which assesses the significance of the percentage of gene clustering in a set of genes based on their genomic positions.²⁷ These results and

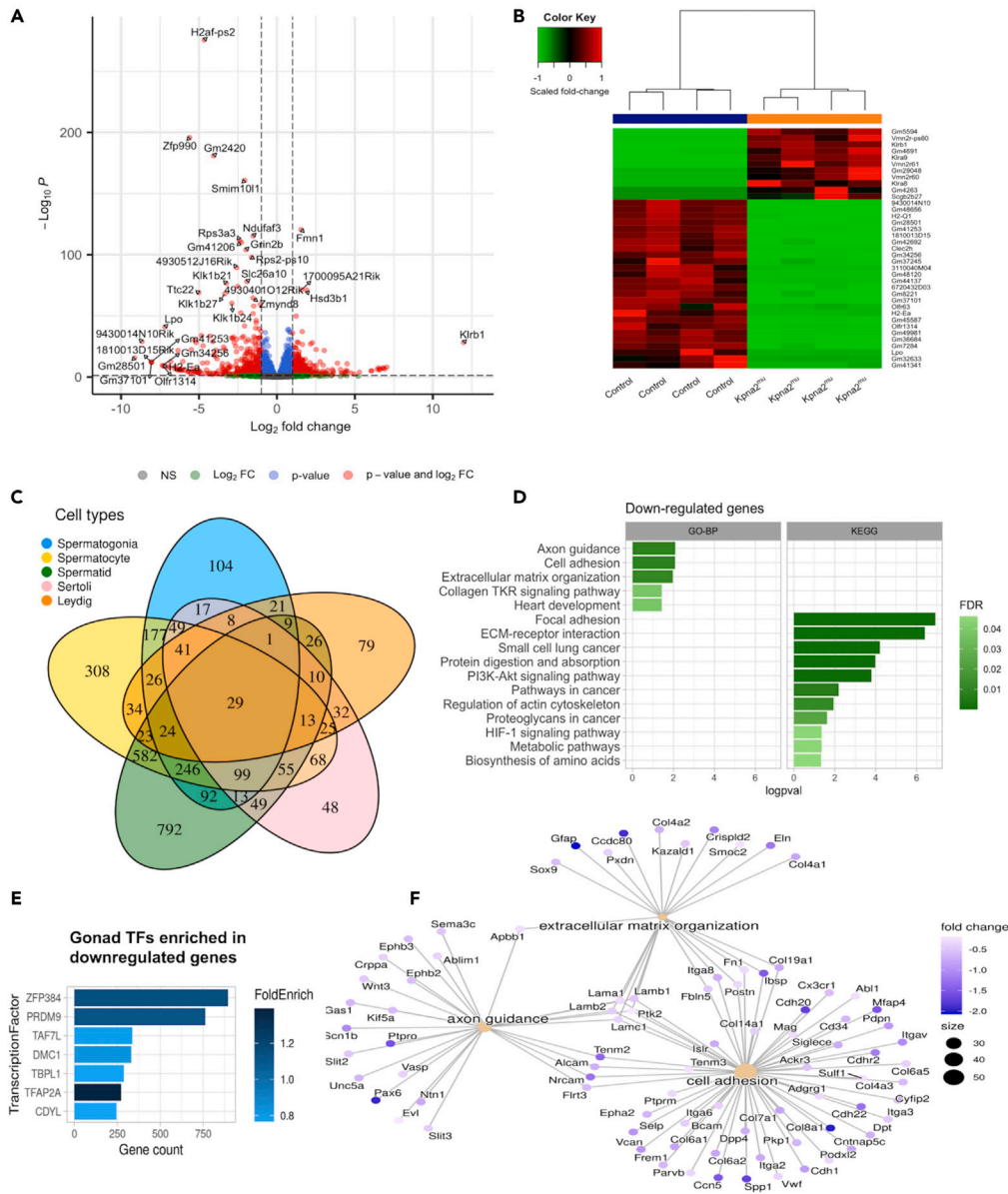


Figure 4. Differential gene expression, ontology, and transcription factor enrichment analysis

(A) Volcano plot summarizing the transcriptional response to the *Kpna2* mutation. The difference in fold change between groups is represented on the x axis and the p value of this difference on the y axis. Genes with an FDR value below 0.05 and a fold change over 2 are indicated in red.

(B) Heatmap of the DEGs showing the greatest difference in fold change (FC > 10) between *Kpna2*^{-/-} and wild-type mice.

(C) Venn diagram of DEG classifications in the different testis cell types including the germ cells (spermatogonia, spermatocyte, and spermatid) and the two major somatic testicular cells (Leydig and Sertoli cells).

(D) Significantly overrepresented biological process terms and KEGG pathways in downregulated genes in the *Kpna2*^{-/-} testes.

(E) Transcription factors that are enriched around the set of downregulated genes identified using the CHIP-Atlas database. The gene count appears on the x axis and fold enrichment as a color gradient.

(F) Top 3 significantly enriched biological process terms in downregulated genes and their associated DEGs. The size of the term nodes depends on the number of DEGs involved in the process, while the color of the gene nodes depends on the difference between the two conditions.

figures showing chromosomes with clusters of 5 or more genes can be found in [Table S3](#). The uniformity test using a p value of 0.05 revealed that downregulated genes were non-uniformly distributed at chromosomes 2, 6, 7, and 9 and up-regulated genes grouped at chromosomes 2, 6, 7, 9, 14, 16, 18, and 19 ([Table S3](#)). With a max-gap of 10, 79.14% of the downregulated genes clustered with a p value of 1.19×10^{-4} while 77.04% of the upregulated genes were grouped with a p value of 3.86×10^{-4} . This indicates there was a significant number of gene clusters in our set of genes with respect to the proportion of gene clusters in the genome. The NKC genomic region at chromosome 6 described above is an example of the gene clustering observed. This region shows two clusters as different genes of the complex were differentially dysregulated (up or down). Another family of closely positioned genes that were found dysregulated is the family of kallikrein-related peptidases (*Klk1b27*, *Klk1b21*, *Klk1b22*, *Klk1b24*, *Klk1*) ([Table S3](#)).

We should highlight that also varying widely between KOs and controls was a set of chemoreceptors, comprising olfactory and vomeronasal receptors. This type of G-protein-coupled receptor has been associated with sperm chemotaxis and motility as well as sperm maturation and migration during spermatogenesis.^{28–30} The phenotypic differences in sperm motility could be explained by the dysregulation of this gene family. In total, 29 olfactory receptors and 11 vomeronasal receptors were differentially expressed ([Figure S4C](#)). Those varying the most were *Olf1r1314*, *Olf1r63*, *Olf1r525*, and *Olf1r463* (downregulated) and *Vmn2r61*, *Vmn2r-ps60*, *Vmn2r60*, and *Vmn2r52* (upregulated).

According to the single-cell RNA-seq analysis of Green et al., 2018,³¹ and data from other studies, we classified the set of DEGs into the following testicular cell types according to their normal expression patterns: spermatogonia, spermatocytes, spermatids, the two major somatic testicular cells Sertoli and Leydig, other somatic cells (macrophages, endothelial, innate lymphoid, peritubular myoid cells, and fibroblasts), and spermatozooids ([Table S4](#)). The DEGs were found to predominantly belong to spermatids, followed by spermatocytes ([Figure 4C](#)). In both, upregulated genes outnumbered downregulated genes. In contrast, in spermatogonia, Sertoli, and Leydig cells, downregulated genes were more abundant.

Gene ontology (GO) and Kyoto Encyclopedia of Genes and Genomes (KEGG) pathway enrichment analysis

Our GO and KEGG overrepresentation analyses offered clues about the disrupted mechanisms existing in the KO mice. The results of this complete analysis with the statistically significant categories and their associated genes can be found in [Table S5](#). The functional annotation reveals enriched biological processes mainly for the downregulated genes ([Figures 4D and 4F](#)). A subset of 58 genes participates in cell adhesion processes involving integrins (*Igta2*, *Igta3*, *Itgav*, *Igta6*, and *Igta8*), components of the laminin complex (*Lama1*, *Lamb2*, *Lamb1*, and *Lamc1*), and collagen (*Col4a3*, *Col6a1*, *Col6a2*, *Col6a5*, *Col7a1*, *Col8a1*, *Col14a1*, and *Col19a1*). In line with this, the GO term extracellular matrix (ECM) organization was also enriched. The ECM is essential for supporting Sertoli and germ cell function in the seminiferous epithelium and coordinating cell migration, proliferation, and differentiation.³² Therefore, ECM dysfunction could disrupt the normal course of spermatogenesis. With regard to KEGG pathways, we also observed enrichment in specialized cell adhesion structures named focal adhesions. Focal adhesions anchor cells to the ECM via integrins, which are transmembrane receptors that bind to constituents of the ECM such as laminins and collagens in basement membranes. For instance, *Ptk2*, which codes for FAK (focal adhesion tyrosine kinase), is downregulated and has been described as an important player in coordinating germ cell migration in the testis during spermatogenesis.³³ FAK transduces signals mediated by integrin-based receptors following its activation by ligands found at the ECM. Another downregulated tyrosine kinase is the non-integrin-type receptor for collagen *Ddr1*, which participates in cell proliferation and migration.³⁴ In this regard, there was enrichment in the collagen-activated tyrosine kinase receptor signaling pathway (*Col4a1*, *Col4a2*, *Col4a3*, *Ddr1*, *Col4a5*, *Col1a1*). Closely related to these overrepresented processes and pathways, the cellular components in which the differential gene products seem to be participating were mainly extracellular, namely proteinaceous ECM, extracellular exosome, and ECM ([Figure S4D](#)), supporting the notion that *Kpna2* could play a role in cell adhesion and migration functions.

Transcription factor binding enrichment

Because of the absence of KPNA2 in our transgenic mice, we considered that some proteins could not be translocated into the nucleus, which may modify transcription factor action, therefore altering the regulation of genes. To dissect the mechanism of dysregulation of protein levels in *Kpna2*^{-/-} testis, we used the chromatin immunoprecipitation sequencing (ChIP-seq) datasets in the ChIP-Atlas platform,³⁵ which searches for proteins significantly bound around multiple query genes. In particular, we looked for the

enrichment of transcription factors that bind to the regions around the DEGs. This could help unveil the regulatory mechanisms behind the gene expression imbalance observed. Our ChIP-Atlas enrichment results are detailed in [Table S6](#).

While upregulated genes showed no significant overrepresentation of transcription factor binding, we found 154 proteins that were enriched around the transcription start sites of downregulated genes. The transcription factors found to be enriched in downregulated genes were mainly those of the pluripotent stem cell experiments, particularly embryonic stem cells, and in only less than 1% of the gonad cell class experiments. Among these enriched transcription factors, we identified the master regulators of embryonic stem cells NANOG, POU5F1, and SOX2. Thus, *Kpna2* seems to modulate certain genes related to pluripotency, which is in agreement with the described role of importins in maintaining stem cells.¹ Remarkably, apart from stem cells, there was enrichment of several transcription factors which are known to be specific or have an important role in the testis, namely: TAF7L (TATA-Box-Binding Protein Associated Factor 7 Like), TBPL1 (TATA-Box-Binding Protein Like 1), ZFP384 (Zinc Finger Protein 384), PRDM9 (PR domain containing 9), DMC1 (DNA meiotic recombinase 1), TFAP2A (Transcription Factor AP-2 Alpha), and CDYL (Chromodomain Y Like) ([Figure 4E](#)). These factors contribute to the transcriptional machinery in the testis and modulate specific processes during spermatogenesis such that their presence in the nucleus is critical in the process of male germ cell differentiation.^{36,37}

Additionally, we analyzed the aminoacidic sequence by using cNLS (classical nuclear localization signal) mapper³⁸ to predict the presence of importin α -dependent nuclear localization signals. We found bipartite NLS in *Taf7l*, *Cdyl*, and *Tbpl1* and monopartite NLS in *Zfp384* ([Table S7](#)). These transcription factors are more likely to be dependent on the α -importome.

Subcellular localization of transcription factors in *Kpna2*^{-/-} testes

To examine the localization of the transcription factors that appear to be altering gene expression as a result of the absence of KPNA2, we performed immunohistochemistry of ZFP384, TBPL1, PRDM9, and TAF7L on stage VIII of the testis seminiferous epithelial cycle of spermatogenesis. We found differences in the signal of the transcription factors between KO and WT testes that indicate they are not being translocated into the nucleus. As shown in [Figure 5](#), ZFP384, which is present in the nucleus of WT spermatocytes as well as round spermatids, is absent in the nucleus of *Kpna2*^{-/-} where it accumulates in the cytoplasm. A similar pattern of subcellular distribution is observed for TBPL1, which remains in the cytoplasm of germ cells lacking KPNA2 ([Figure 6](#)). In WT testis, the signal of PRDM9 is observed in the nucleus of round spermatids which is lost in *Kpna2*^{-/-} cells ([Figure 7](#)). In the case of TAF7L, in normal conditions, it is present in round and elongated spermatids ([Figure 8](#)). Interestingly, in the KO spermatids, but not in the WT, both PRDM9 and TAF7L seem to be located at the acrosome besides some cytoplasmic signal ([Figures 7 and 8](#)). These differences observed in PRDM9 and TAF7L could be due to a reduced expression at the protein level rather than altered transport to the nucleus. Therefore, the expression level of both proteins was measured by western blotting after subcellular fractionation to obtain their expression in nucleus and cytoplasm of WT and KO testes. Differences in the total protein amount between the WT and KO testes, represented as integrated area/ μg , were not significant for both factors ($p > 0.05$) ([Figures S5A–S5B](#)). However, proteins were measured in whole testis samples, which could be masking the effect on spermatids.

Our findings support the role of *Kpna2* in regulating the entrance of transcription factors that control the timely gene expression necessary at the different stages of spermatogenesis.

Structural homology of KPNA2 with the α -importins expressed in testis

FATCAT (Flexible structure AlignmentT by Chaining Aligned fragment pairs allowing Twists) alignment between KPNA2 and the importins expressed in testis, which are KPNA1, KPNA6, KPNA3, and KPNA4, revealed the highest score between KPNA2 and KPNA3 followed by KPNA4. Both belong to the same family. [Table S8](#) shows these results, where all comparisons were significant with p values of 0, as they are part of the same family. This similarity in the structures is displayed in [Figure S6](#). The structural similarity with other importins can help assess the specificity and compensation of the translocation of the potential cargoes.

DISCUSSION

Here we describe the generation of a *Kpna2* null allele through CRISPR-Cas9-mediated genome editing. Homozygous male mice lacking functional *Kpna2* feature normal testis determination, normal adult mutant

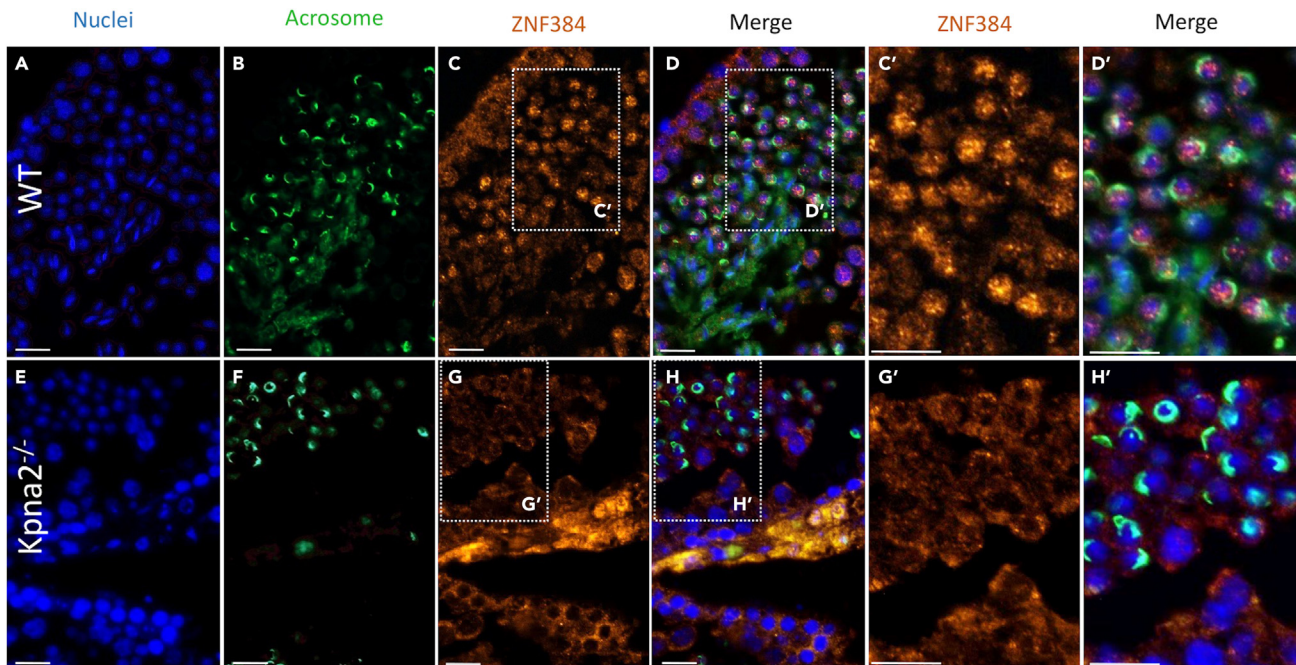


Figure 5. Distribution of ZFP384 in tubules seminiferous of wild-type and *Kpna2*^{-/-} mice

Representative images of cross-sections of seminiferous tubules stained with (A, E) Hoechst (blue), (B, F) FITC-PNA (green), (C, G) anti-ZNF384 (orange), and (D, H) merged images. C' and G' are amplification of the images in the rectangle of C and G, showing that in WT testes ZFP384 is located in the nucleus of round spermatids but in *Kpna2*^{-/-} spermatids ZFP384 is located in the cytoplasm of the spermatids. D' and H' are amplification of the same areas of merged images D and H, showing that in WT nucleus are pink (blue color that represents nucleus staining by Hoechst + orange color that indicates ZNF384 proteins) and in *Kpna2*^{-/-} nucleus are only blue. Scale bar: 100 μ m.

testis size, and normal histology yet show a reduced body size and abnormal sperm morphology and motility producing completely infertile males. These mice exhibit testes transcriptomic dysregulation affecting clusters of genes related to adhesion proteins, integrins, components of the ECM, and several gene complexes and families, such as the olfactory receptors which have been associated with sperm chemotaxis.²⁸ This modified gene expression could be mediated by the impaired translocation of testis-specific transcription factors that control the expression of these genes which could be leading to abnormal sperm and infertility.

Kpna2 is the main importin α expressed in the placenta and during embryonic testis development, sex determination, and spermatogenesis.^{24,39} Our *Kpna2*-KO mice were born in smaller litters than expected and were smaller than normal, indicating that *Kpna2* function is only partially compensated during fetal development. KOs also undergo normal testes development and differentiation, indicating that another importin α takes over this function in these processes. However, some specific *Kpna2* functions cannot be replaced especially during spermatogenesis, producing an abnormal sperm morphology and motility and consequently causing infertility. Our immunofluorescence analysis indicates that the expression of KPNA2 is cytoplasmic in spermatogonia and primary spermatocytes and both nuclear and cytoplasmic in pachytene spermatocytes and spermatids, suggesting a dual function of *Kpna2* in the testis. Previous studies differ in these observations, owing to their use of different antibodies. Miyamoto et al.¹⁷ report the presence of KPNA2 in the rat testis in the cytoplasm of pachytene spermatocytes, spermatids, and Leydig cells and the nucleus of pachytene spermatocytes, while Ly-Huynh et al.²⁶ detected KPNA2 in the nucleus of pachytene spermatocytes, the cytoplasm of round spermatids, and nucleus and cytoplasm in elongating spermatids. However, they all agree that there is a strong signal of KPNA2 in spermatocytes and spermatids. When KPNA2 is only present in the cytoplasm, it can anchor proteins in the cytoplasm; however, when present in both nucleus and cytoplasm, it could be working as a nucleocytoplasmic transporter or as a regulator of gene expression in association with chromatin.⁴⁰ The fact that in *Kpna2*-KO mice the number of produced spermatozoa is not affected indicates that KPNA2 is not essential until the protein is present in the nucleus at pachytene spermatocyte and spermatid stages, suggesting that at these stages

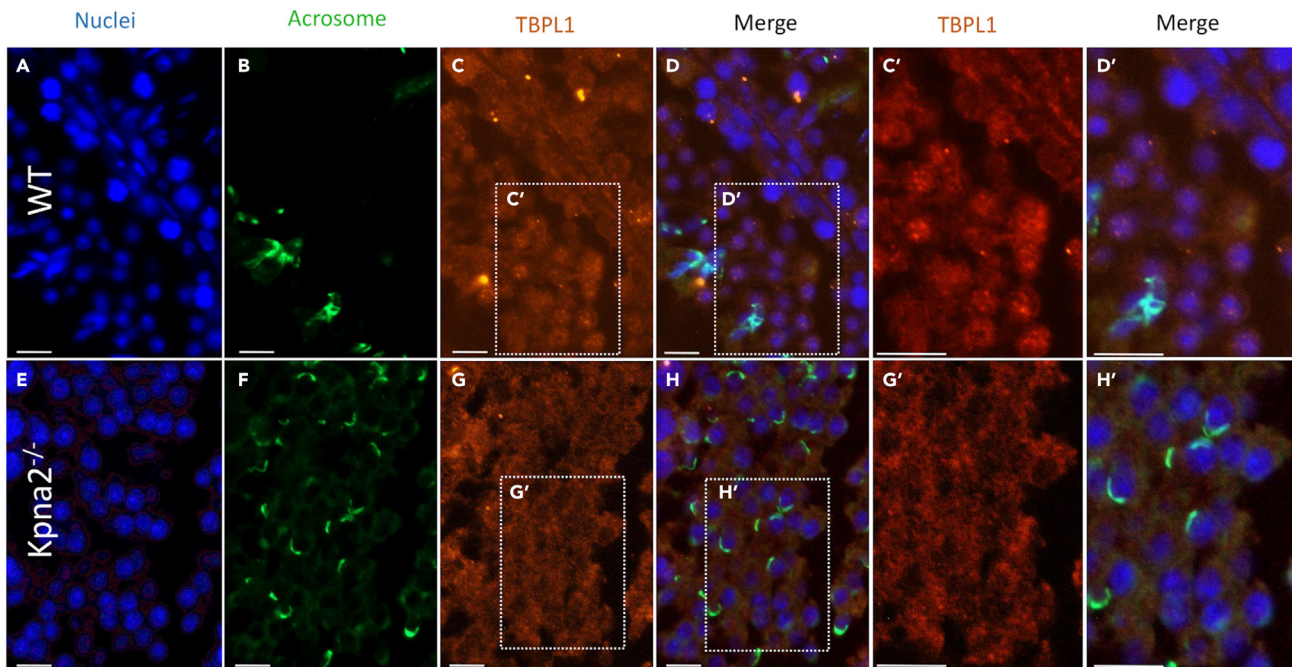


Figure 6. Distribution of TBPL1 in tubules seminiferous of wild-type and *Kpna2*^{-/-} mice

Representative images of cross-sections of seminiferous tubules stained with (A, E) Hoechst (blue), (B, F) FITC-PNA (green), (C, G) anti-TBPL1 (orange), and (D, H) merged images. C' and G' are amplification of the images in the rectangle of C and G, showing that in WT testes TBPL1 is located in the nucleus of round spermatids but in *Kpna2*^{-/-} spermatids TBPL1 is located in the cytoplasm of the spermatids. D' and H' are amplification of the same areas of merged images D and H, showing that in WT nucleus are pink (blue color that represents nucleus staining by Hoechst + orange color that indicates ZNF384 proteins) and in *Kpna2*^{-/-} nucleus are only blue. Scale bar: 100 μ m.

its function may not be compensated by other importin α s. In agreement with this, we found that most DEGs occurred in spermatocytes and spermatids. This means it was the blocked nucleocytoplasmic transport or nuclear functions in the KOs during late spermatogenesis that produced the phenotypic effects.

Different importin α s have different cargo specificities. In terms of the importance of *Kpna2* for fertile sperm production, KPNA2 is proposed to have binding selectivity for transcription or epigenetic factors with specific functions in spermatocytes and spermatids. Hence the genetic loss of *Kpna2* may block the transport of essential factors to the nucleus, therefore disrupting the specialized mechanisms that drive spermiogenesis. In line with this, we identified testes transcription factors showing over-representative binding in the genes that were less expressed upon loss of KPNA2, which could mean the impaired transport of these essential transcriptional activators to the nucleus.

The first transcription factor that was more enriched was ZFP384, also called NMP4 (nuclear matrix protein 4), a nucleocytoplasmic shuttling transcription factor that regulates the expression of collagen and matrix metalloproteinases.⁴¹ *Zfp384*-KO mice tend to be smaller than WT mice, and spermatogenic cell degeneration produces infertility in some of these mice.³⁶ The second transcription factor found enriched was PRDM9, a gene only expressed in the testis that codes for a zinc-finger protein with histone methyltransferase activity. This protein catalyzes histone H3 lysine 4 trimethylation (H3K4me3) during meiotic prophase. H3K4me3 is commonly associated with activating the transcription of nearby genes related to development and establishing cell identity.⁴² *Prdm9*-deficient mice are infertile and feature aberrant synapsis and apparent impairment of DNA double-strand break (DSB) repair in spermatocytes.⁴³ Another enriched transcription factor detected here was TAF7L, a component of the TFIID (transcription factor IID) required for the transcription of most protein-coding genes by RNA polymerase II. TAF7L is a paralog of TAF7, which is specific to male germ cell development in mice.⁴⁴ As germ cell development progresses, TAF7L expression increases and TAF7 expression diminishes. TAF7L is expressed after meiosis at a dynamically regulated intracellular localization.⁴⁴ This transcription factor binds to promoters of activated post-meiotic genes in the testis, and *Taf7l*-KO mice display no spermatogenic arrest but abnormal sperm

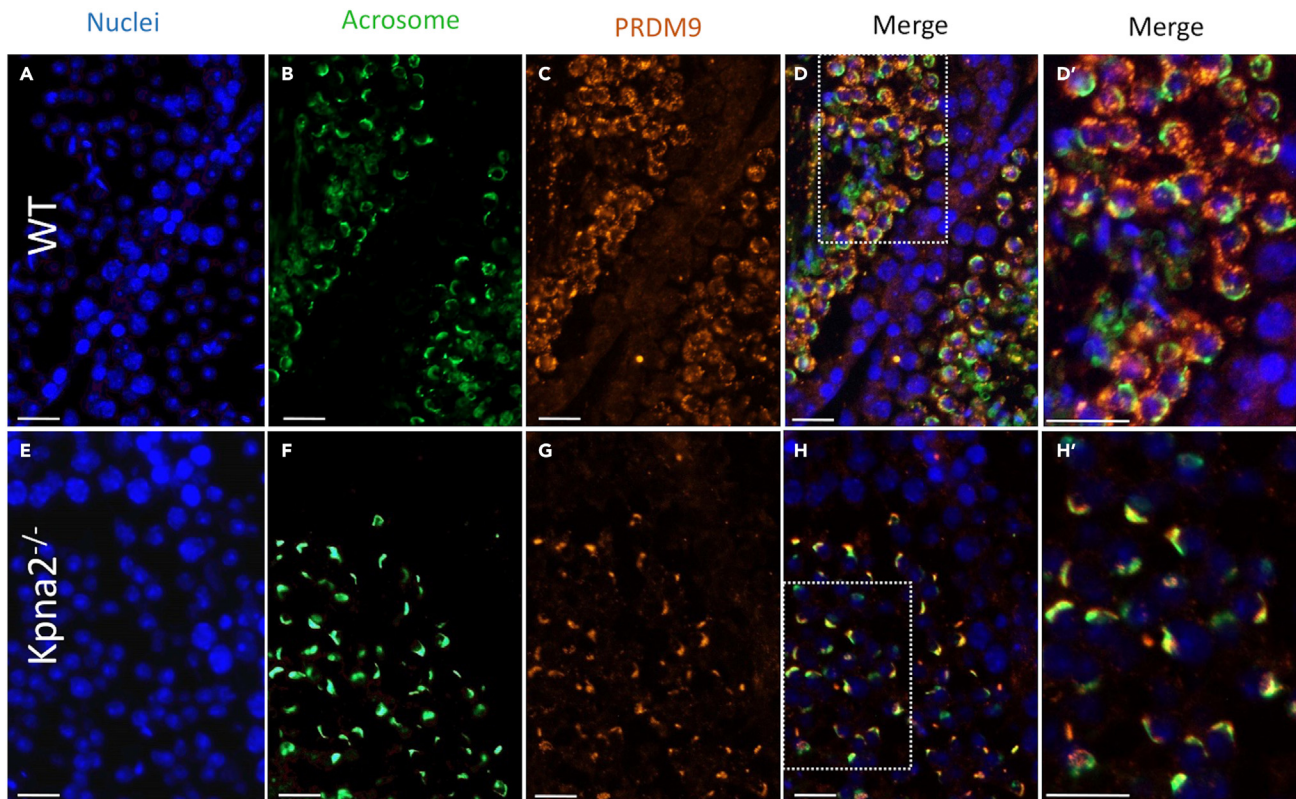


Figure 7. Distribution of PRDM9 in tubules seminiferous of wild-type and *Kpna2*^{-/-} mice
Representative images of cross-sections of seminiferous tubules stained with Hoechst (blue) (A, E), FITC-PNA (green) (B, F), anti-PRDM9 (orange) (C, G), and (D, H) merged images. D' and H' are amplification of the images in the rectangle of D and H, showing that in WT PRDM9 is located in the nucleus and around the nucleus of round spermatids but in *Kpna2*^{-/-} spermatids PRDM9 is located in the acrosome. Scale bar: 100 μ m.

morphology and motility, with differences in velocity parameters similar to our mutants. As well, mutations in *Taf7l* might play a role in oligozoospermia in men.^{44,45} Another binding factor potentially translocated by KPNA2 is DMC1, which is expressed specifically in the testis and has been described to regulate homologous recombination defects in pachytene spermatocytes. Male and female *Dmc1*-KO mice are infertile.⁴⁶ Another transcription factor identified is TBPL1, a gene specific to testis that encodes a member of the TATA-box-binding protein family, which plays a critical role in transcription by RNA polymerase II. *Tbp1* plays a critical role in spermatogenesis, and its complete absence leads to the arrest of spermiogenesis.³⁷ TBPL1 is recruited to active haploid cell promoters together with TAF7L and RNA polymerase II. A set of genes activated in haploid spermatids during the first wave of spermatogenesis has been identified, whose expression is downregulated by *Tbp1* inactivation, suggesting a critical role of *Tbp1* in haploid cell gene expression.⁴⁷ A further binding factor potentially translocated by KPNA2 is CDYL which is expressed only in the testis. Deletion of *Cdyl* in mice leads to a reduction of sperm motility,⁴⁸ as well as defects in spermatogenesis maintenance and spermatozoon morphogenesis, producing teratozoospermia and a progressive infertility phenotype in adulthood.⁴⁹

Considering the phenotypic effects of the deletion of TFs (transcription factors), the transport of ZFP384, PRDM9, TBPL1, and DMC1 could be compensated by other importins. However, TAF7L and CYDL KOs exhibit a similar phenotype as *Kpna2* KOs, which could indicate a binding preference of KPNA2 to these factors. In addition, we found potential importin α -dependent NLS motifs in both transcription factors which supports the fact that these TFs could be translocated by an α -importin mechanism.

Remarkably, the factors described above show a similar subcellular localization as KPNA2. Some of these proteins may be transported to the nucleus by other mechanisms, but the loss of *Kpna2* has a clear effect of reducing the expression of genes to which these factors bind, leading to the general dysregulation of the

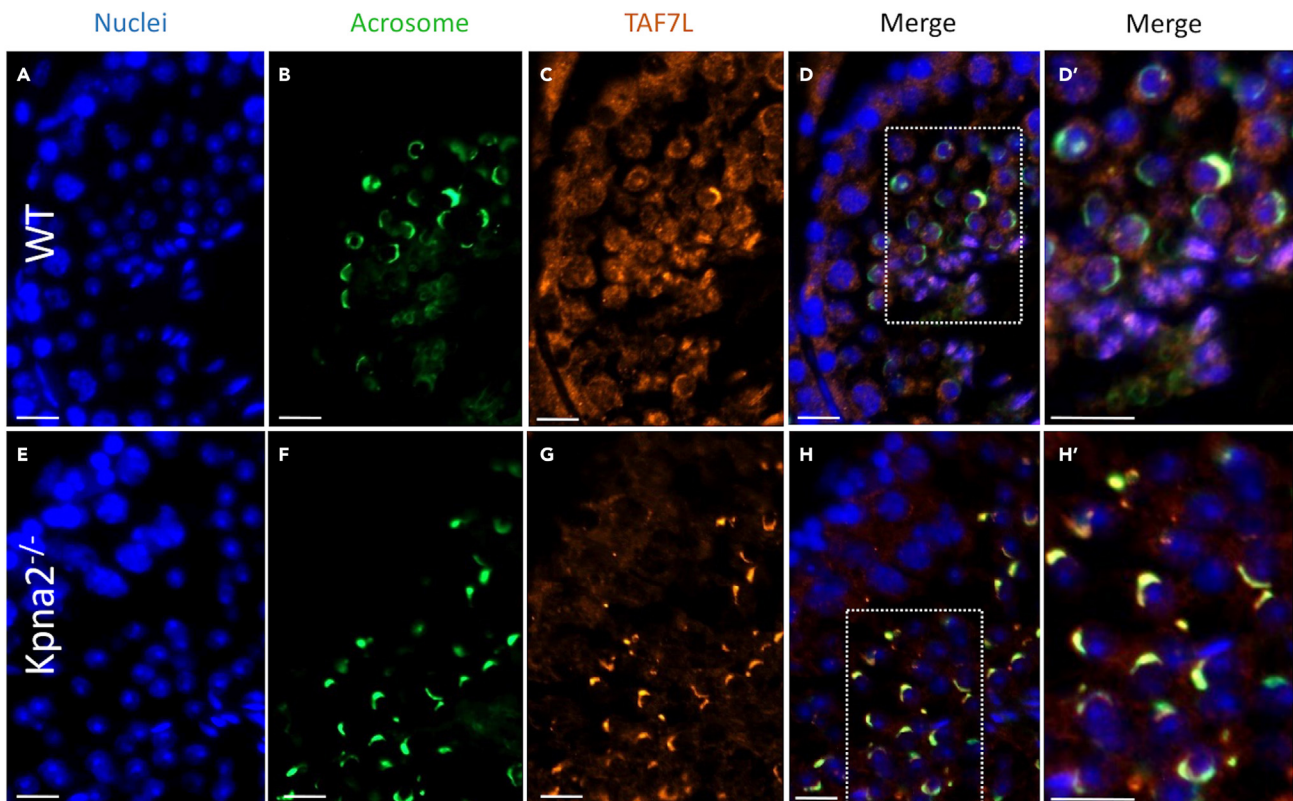


Figure 8. Distribution of TAF7L in tubules seminiferous of wild-type and *Kpna2*^{-/-} mice

Representative images of cross-sections of seminiferous tubules stained with Hoechst (blue) (A, E), FITC-PNA (green) (B, F), anti-TAF7L (orange) (C, G), and (D, H) merged images. D' and H' are amplification of the images in the rectangle of D and H, showing that in WT TAF7L is located in the nucleus of round and elongated spermatids (nucleus are pink: blue color that represents nucleus staining by Hoechst + orange color that indicates TAF7L proteins) but in *Kpna2*^{-/-} TAF7L is located in acrosome. Scale bar: 100 μ m.

intricate networks that participate in male gamete formation. As previously described, the nucleocytoplasmic transport of these transcription factors is critical for the progression of spermatogenesis. Importins exert their function in a tissue- and cell-type-specific manner, and each α -importin has different NLS binding specificities. However, the transport of certain factors may be compensated by other α -importins in the absence of *Kpna2*. Of the six mouse α -importins, apart from *Kpna2* other 4 are expressed in the testis (*Kpna1*, *Kpna3*, *Kpna4*, and *Kpna6*),⁵⁰ and in particular, at the spermatocyte and spermatid stage. Mammalian importins are classified based on sequence homology in 3 subtypes: α P, α S, and α Q.^{50,51} *Kpna2* belongs to the α P clade together with *Kpna7*, not observed in testis, so among the testis-expressed α -importins, KPNA2 may have different specificities than the rest which belong to the α S and α Q clades. Furthermore, the structural similarity analysis identified KPNA3 as the most similar importin followed by KPNA4. Although *Kpna3* is not essential for spermatogenesis, *Kpna4*^{-/-} mice exhibit subfertility features.¹⁴ The function of KPNA2 may be partially compensated by these importins. In fact, KPNA3 and KPNA4 have been reported to bind to ZFP384 in rats,¹⁷ whose entry to the nucleus therefore may be facilitated by these in the absence of KPNA2. This is also in accordance with the phenotypic differences between *Zfp384* KO and our KOs.

Altogether, we report that the translocation of the transcription factors without KPNA2 is not enough to maintain the normal transcriptional program and produce fertile sperm. Besides a nuclear import role, KPNA2 may also act in the nucleus of late spermatocytes and spermatids by associating with chromatin via its direct DNA-binding ability, promoting gene expression. This feature, which has been examined in embryonic stem cells,⁴⁰ should be further explored to determine whether KPNA2 binds to DNA in spermatogenic cells. Whether through the regulation of transcription factors transported to the nucleus or through the control of expression due to its direct association with chromatin, KPNA2 was observed here to exert a specific control of the expression of gene clusters present in certain chromosomes. Our

findings point to KPNA2 as a pivotal importin in the process of sperm production through its unique function. This importin thus emerges as a key mediator of nucleocytoplasmic transport of transcription factors specific to spermatogenesis.

Limitations of the study

We have described the phenotypic and molecular consequences of the loss of *Kpna2* in the seminiferous tubules. To decipher the mechanism of the importin, RNA-seq analysis helped to identify possible cargoes of *Kpna2* along spermatogenesis. Thanks to the immunohistochemical assays, we observed differences in the subcellular localization of the transcription factors in the KO testes. However, further experimental validation is required to confirm the interaction of *Kpna2* with the proposed transcription factors, as well as the extent to which this is the only cause of underlying fertility. As well, *Kpna2* may be participating in additional molecular functions other than nuclear import, which have not been explored here.

STAR★METHODS

Detailed methods are provided in the online version of this paper and include the following:

- KEY RESOURCES TABLE
- RESOURCE AVAILABILITY
 - Lead contact
 - Materials availability
 - Data and code availability
- EXPERIMENTAL MODEL AND SUBJECT DETAILS
 - *Kpna2*-KO mice
- METHOD DETAILS
 - Sperm collection
 - Sperm morphology
 - Sperm motility analysis
 - Gonadosomatic index
 - Intracytoplasmic sperm injection (ICSI) and in vitro fertilization (IVF)
 - Western blots
 - Immunohistochemistry
 - TUNEL-assay
 - RNA-seq analysis
 - Differential gene expression and functional characterization
 - Classification of genes according to their expression in the different testis cell types
 - Structural pairwise alignment
- QUANTIFICATION AND STATISTICAL ANALYSIS

SUPPLEMENTAL INFORMATION

Supplemental information can be found online at <https://doi.org/10.1016/j.isci.2023.107134>.

ACKNOWLEDGMENTS

This research was supported by Grants RTI2018-093548-B-I00 and PID2021-122507OB-I00 funded by MCIN/AEI/10.13039/501100011033/and European Union "NextGenerationEU"/PRTR). P.N was supported by a pre-doctoral fellowship from the Spanish Ministry of Science and Innovation (MICINN) (PRE2019-088813), and M.L was supported by a Juan de la Cierva postdoctoral contract (FJC2019-040385-I) from the MICINN. We gratefully thank CESGA (Supercomputing Center of Galicia) for providing the necessary resources for the data processing.

AUTHOR CONTRIBUTIONS

P.N. performed the bioinformatics analysis and wrote the manuscript. M.M. analyzed mice phenotype and performed sperm analysis and western blot. M.L and E.P. performed the immunohistochemical assays. R.F.G. and P.R.-I. produced both transgenic constructs and mice. A.G.-A. conceived this project, supervised the study, and wrote the manuscript.

DECLARATION OF INTERESTS

The authors declare no competing interests.

Received: December 20, 2022

Revised: March 16, 2023

Accepted: June 12, 2023

Published: June 16, 2023

REFERENCES

- Yasuhara, N., and Yoneda, Y. (2017). Importins in the maintenance and lineage commitment of ES cells. *Neurochem. Int.* 105, 32–41. <https://doi.org/10.1016/j.neuint.2017.01.020>.
- Teng, S.C., Wu, K.J., Tseng, S.F., Wong, C.W., and Kao, L. (2006). Importin KPNA2, NBS1, DNA repair and tumorigenesis. *J. Mol. Histol.* 37, 293–299. <https://doi.org/10.1007/S10735-006-9032-Y>.
- Umegaki, N., Tamai, K., Nakano, H., Moritsugu, R., Yamazaki, T., Hanada, K., Katayama, I., and Kaneda, Y. (2007). Differential regulation of karyopherin alpha 2 expression by TGF-beta1 and IFN-gamma in normal human epidermal keratinocytes: evident contribution of KPNA2 for nuclear translocation of IRF-1. *J. Invest. Dermatol.* 127, 1456–1464. <https://doi.org/10.1038/SJ.JID.5700716>.
- Yasuhara, N., Shibasaki, N., Tanaka, S., Nagai, M., Kamikawa, Y., Oe, S., Asally, M., Kamachi, Y., Kondoh, H., and Yoneda, Y. (2007). Triggering neural differentiation of ES cells by subtype switching of importin-alpha. *Nat. Cell Biol.* 9, 72–79. <https://doi.org/10.1038/NCB1521>.
- Hall, M.N., Griffin, C.A., Simionescu, A., Corbett, A.H., and Pavlath, G.K. (2011). Distinct roles for classical nuclear import receptors in the growth of multinucleated muscle cells. *Dev. Biol.* 357, 248–258. <https://doi.org/10.1016/j.ydbio.2011.06.032>.
- Yasuhara, N., Oka, M., and Yoneda, Y. (2009). The role of the nuclear transport system in cell differentiation. *Semin. Cell Dev. Biol.* 20, 590–599. <https://doi.org/10.1016/j.semcdb.2009.05.003>.
- Yasuda, Y., Miyamoto, Y., Yamashiro, T., Asally, M., Masui, A., Wong, C., Loveland, K.L., and Yoneda, Y. (2012). Nuclear retention of importin α coordinates cell fate through changes in gene expression. *EMBO J.* 31, 83–94. <https://doi.org/10.1038/EMBOJ.2011.360>.
- Jibiki, K., Kodama, T.S., Suenaga, A., Kawase, Y., Shibasaki, N., Nomoto, S., Nagasawa, S., Nagashima, M., Shimodan, S., Kikuchi, R., et al. (2021). Importin $\alpha 2$ association with chromatin: Direct DNA binding via a novel DNA-binding domain. *Gene Cell.* 26, 945–966. <https://doi.org/10.1111/gtc.12896>.
- Gruss, O.J., Carazo-Salas, R.E., Schatz, C.A., Guarguaglini, G., Kast, J., Wilm, M., Le Bot, N., Vernos, I., Karsenti, E., and Mattaj, I.W. (2001). Ran Induces Spindle Assembly by Reversing the Inhibitory Effect of Importin α on TPX2 Activity. *Cell* 104, 83–93. [https://doi.org/10.1016/S0092-8674\(01\)00193-3](https://doi.org/10.1016/S0092-8674(01)00193-3).
- Hachet, V., Köcher, T., Wilm, M., and Mattaj, I.W. (2004). Importin alpha associates with membranes and participates in nuclear envelope assembly in vitro. *EMBO J.* 23, 1526–1535. <https://doi.org/10.1038/SJ.EMBOJ.7600154>.
- Shao, X., Kawauchi, K., Shivashankar, G.V., and Bershadsky, A.D. (2015). Novel localization of formin mDia2: importin β -mediated delivery to and retention at the cytoplasmic side of the nuclear envelope. *Biol. Open* 4, 1569–1575. <https://doi.org/10.1242/BIO.013649/-/DC1>.
- Christiansen, A., and Dyrsjø, L. (2013). The functional role of the novel biomarker karyopherin $\alpha 2$ (KPNA2) in cancer. *Cancer Lett.* 331, 18–23. <https://doi.org/10.1016/j.canlet.2012.12.013>.
- Perry, R.B.T., and Fainzilber, M. (2009). Nuclear transport factors in neuronal function. *Semin. Cell Dev. Biol.* 20, 600–606. <https://doi.org/10.1016/j.semcdb.2009.04.014>.
- Miyamoto, Y., Sasaki, M., Miyata, H., Monobe, Y., Nagai, M., Otani, M., Whiley, P.A.F., Morohoshi, A., Oki, S., Matsuda, J., et al. (2020). Genetic loss of importin $\alpha 4$ causes abnormal sperm morphology and impacts on male fertility in mouse. *Faseb J.* 34, 16224–16242. <https://doi.org/10.1096/FJ.202000768RR>.
- Hu, J., Wang, F., Yuan, Y., Zhu, X., Wang, Y., Zhang, Y., Kou, Z., Wang, S., and Gao, S. (2010). Novel importin- α family member Kpna7 is required for normal fertility and fecundity in the mouse. *J. Biol. Chem.* 285, 33113–33122. <https://doi.org/10.1074/jbc.M110.117044>.
- Mihalas, B.P., Western, P.S., Loveland, K.L., McLaughlin, E.A., and Holt, J.E. (2015). Changing expression and subcellular distribution of karyopherins during murine oogenesis. *Reproduction* 150, 485–496. <https://doi.org/10.1530/REP-14-0585>.
- Miyamoto, Y., Baker, M.A., Whiley, P.A., Arjomand, A., Ludeman, J., Wong, C., Jans, D.A., and Loveland, K.L. (2013). Towards delineation of a developmental α -importome in the mammalian male germline. *Biochim. Biophys. Acta* 1833, 731–742. <https://doi.org/10.1016/j.bbamcr.2012.11.005>.
- Loveland, K.L., Major, A.T., Butler, R., Young, J.C., Jans, D.A., and Miyamoto, Y. (2015). Putting things in place for fertilization: discovering roles for importin proteins in cell fate and spermatogenesis. *Asian J. Androl.* 17, 537–544. <https://doi.org/10.4103/1008-682X.154310>.
- Arjomand, A., Baker, M.A., Li, C., Buckle, A.M., Jans, D.A., Loveland, K.L., and Miyamoto, Y. (2014). The α -importome of mammalian germ cell maturation provides novel insights for importin biology. *Faseb J.* 28, 3480–3493. <https://doi.org/10.1096/FJ.13-244913>.
- Moriyama, T., Nagai, M., Oka, M., Ikawa, M., Okabe, M., and Yoneda, Y. (2011). Targeted disruption of one of the importin α family members leads to female functional incompetence in delivery. *FEBS J.* 278, 1561–1572. <https://doi.org/10.1111/j.1742-4658.2011.08079.x>.
- Liu, N., Qadri, F., Busch, H., Huegel, S., Sihm, G., Chuykin, I., Hartmann, E., Bader, M., and Rother, F. (2021). Kpna6 deficiency causes infertility in male mice by disrupting spermatogenesis. *Dev* 148, dev198374. <https://doi.org/10.1242/DEV.198374>.
- Rother, F., Schmidt, T., Popova, E., Krivokharchenko, A., Hügel, S., Vilianovich, L., Ridders, M., Tenner, K., Alenina, N., Köhler, M., et al. (2011). Importin $\alpha 7$ Is Essential for Zygotic Genome Activation and Early Mouse Development. *PLoS One* 6, e18310. <https://doi.org/10.1371/JOURNAL.PONE.0018310>.
- Young, J.C., Ly-Huynh, J.D., Lescesen, H., Miyamoto, Y., Browne, C., Yoneda, Y., Koopman, P., Loveland, K.L., and Jans, D.A. (2013). The nuclear import factor importin $\alpha 4$ can protect against oxidative stress. *Biochim. Biophys. Acta* 1833, 2348–2356. <https://doi.org/10.1016/j.bbamcr.2013.06.007>.
- Major, A.T., Whiley, P.A.F., and Loveland, K.L. (2011). Expression of nucleocytoplasmic transport machinery: Clues to regulation of spermatogenic development. *Biochim. Biophys. Acta* 1813, 1668–1688. <https://doi.org/10.1016/j.bbamcr.2011.03.008>.
- Ly-Huynh, J.D., Lieu, K.G., Major, A.T., Whiley, P.A.F., Holt, J.E., Loveland, K.L., and Jans, D.A. (2011). Importin Alpha2-Interacting Proteins with Nuclear Roles During Mammalian Spermatogenesis. *Biol. Reprod.* 85, 1191–1202. <https://doi.org/10.1095/BIOLREPROD.111.091686>.
- Wang, C.I., Chien, K.Y., Wang, C.L., Liu, H.P., Cheng, C.C., Chang, Y.S., Yu, J.S., and Yu, C.J. (2012). Quantitative proteomics reveals regulation of karyopherin subunit alpha-2 (KPNA2) and its potential novel cargo proteins in nonsmall cell lung cancer. *Mol.*

- Cell. Proteomics 11, 1105–1122. <https://doi.org/10.1074/MCP.M111.016592>.
27. Pazos Obregón, F., Soto, P., Lavín, J.L., Cortázar, A.R., Barrio, R., Aransay, A.M., and Cantera, R. (2018). Cluster Locator, online analysis and visualization of gene clustering. *Bioinformatics* 34, 3377–3379. <https://doi.org/10.1093/BIOINFORMATICS/BTY336>.
 28. Spehr, M., Schwane, K., Riffell, J.A., Zimmer, R.K., and Hatt, H. (2006). Odorant receptors and olfactory-like signaling mechanisms in mammalian sperm. *Mol. Cell. Endocrinol.* 250, 128–136. <https://doi.org/10.1016/j.mce.2005.12.035>.
 29. Fukuda, N., and Touhara, K. (2006). Developmental expression patterns of testicular olfactory receptor genes during mouse spermatogenesis. *Gene Cell.* 11, 71–81. <https://doi.org/10.1111/J.1365-2443.2005.00915.X>.
 30. Milardi, D., Colussi, C., Grande, G., Vincenzoni, F., Pierconti, F., Mancini, F., Baroni, S., Castagnola, M., Marana, R., and Pontecorvi, A. (2017). Olfactory receptors in semen and in the male tract: From proteome to proteins. *Front. Endocrinol.* 8, 379. <https://doi.org/10.3389/FENDO.2017.00379/BIBTEX>.
 31. Green, C.D., Ma, Q., Manske, G.L., Shami, A.N., Zheng, X., Marini, S., Moritz, L., Sultan, C., Gurczynski, S.J., Moore, B.B., et al. (2018). A Comprehensive Roadmap of Murine Spermatogenesis Defined by Single-Cell RNA-Seq. *Dev. Cell* 46, 651–667. <https://doi.org/10.1016/j.devcel.2018.07.025>.
 32. Siu, M.K.Y., and Cheng, C.Y. (2008). Extracellular Matrix and Its Role in Spermatogenesis. *Adv. Exp. Med. Biol.* 636, 74–91. https://doi.org/10.1007/978-0-387-09597-4_5.
 33. Gungor-Ordueri, N.E., Mruk, D.D., Wan, H.T., Wong, E.W.P., Celik-Ozenci, C., Lie, P.P.Y., and Cheng, C.Y. (2014). New insights into FAK function and regulation during spermatogenesis. *Histol. Histopathol.* 29, 977–989. <https://doi.org/10.14670/HH-29.977>.
 34. Vogel, W.F., Abdulhussein, R., and Ford, C.E. (2006). Sensing extracellular matrix: An update on discoidin domain receptor function. *Cell. Signal.* 18, 1108–1116. <https://doi.org/10.1016/j.celsig.2006.02.012>.
 35. Oki, S., Ohta, T., Shioi, G., Hatanaka, H., Ogasawara, O., Okuda, Y., Kawaji, H., Nakaki, R., Sese, J., and Meno, C. (2018). ChIP-Atlas: a data-mining suite powered by full integration of public ChIP-seq data. *EMBO Rep.* 19, e46255. <https://doi.org/10.15252/EMBR.201846255>.
 36. Nakamoto, T., Shiratsuchi, A., Oda, H., Inoue, K., Matsumura, T., Ichikawa, M., Saito, T., Seo, S., Maki, K., Asai, T., et al. (2004). Impaired spermatogenesis and male fertility defects in Ciz/Nmp4-disrupted mice. *Gene Cell.* 9, 575–589. <https://doi.org/10.1111/J.1356-9597.2004.00746.X>.
 37. Zhang, D., Penttila, T.L., Morris, P.L., Teichmann, M., and Roeder, R.G. (2001). Spermiogenesis deficiency in mice lacking the Trf2 gene. *Science* 292, 1153–1155. https://doi.org/10.1126/SCIENCE.1059188/SUPPL_FILE/1059188S2_THUMB.GIF.
 38. Kosugi, S., Hasebe, M., Tomita, M., and Yanagawa, H. (2009). Systematic identification of cell cycle-dependent yeast nucleocytoplasmic shuttling proteins by prediction of composite motifs. *Proc. Natl. Acad. Sci. USA* 106, 10171–10176. <https://doi.org/10.1073/pnas.0900604106>.
 39. Planells, B., Gómez-Redondo, I., Pericuesta, E., Lonergan, P., and Gutiérrez-Adán, A. (2019). Differential isoform expression and alternative splicing in sex determination in mice. *BMC Genom.* 20, 202. <https://doi.org/10.1186/s12864-019-5572-x>.
 40. Jibiki, K., Kodama, T.S., Suenaga, A., Kawase, Y., Shibazaki, N., Nomoto, S., Nagasawa, S., Nagashima, M., Shimodan, S., Kikuchi, R., et al. (2020). Importin $\alpha 2$ associates with chromatin via a novel DNA binding domain. Pre print at bioRxiv. <https://doi.org/10.1101/2020.05.04.075580>.
 41. Nakamoto, T., Yamagata, T., Sakai, R., Ogawa, S., Honda, H., Ueno, H., Hirano, N., Yazaki, Y., and Hirai, H. (2000). CIZ, a Zinc Finger Protein That Interacts with p130 cas and Activates the Expression of Matrix Metalloproteinases. *Mol. Cell Biol.* 20, 1649–1658. <https://doi.org/10.1128/MCB.20.5.1649-1658.2000/ASSET/AAC0D0AF-4DA5-45EB-AFB2-1B5D1FC8C457/ASSETS/GRAPHIC/MB0501445007.JPEG>.
 42. Bernstein, B.E., Mikkelsen, T.S., Xie, X., Kamal, M., Huebert, D.J., Cuff, J., Fry, B., Meissner, A., Wernig, M., Plath, K., et al. (2006). A Bivalent Chromatin Structure Marks Key Developmental Genes in Embryonic Stem Cells. *Cell* 125, 315–326. <https://doi.org/10.1016/j.cell.2006.02.041>.
 43. Hayashi, K., Yoshida, K., and Matsui, Y. (2005). A histone H3 methyltransferase controls epigenetic events required for meiotic prophase. *Nat* 438, 374–378. <https://doi.org/10.1038/nature04112>.
 44. Pointud, J.C., Mengus, G., Brancorsini, S., Monaco, L., Parvinen, M., Sassone-Corsi, P., and Davidson, I. (2003). The intracellular localisation of TAF7L, a paralogue of transcription factor TFIID subunit TAF7, is developmentally regulated during male germ-cell differentiation. *J. Cell Sci.* 116, 1847–1858. <https://doi.org/10.1242/JCS.00391>.
 45. Cheng, Y., Buffone, M.G., Kouadio, M., Goodheart, M., Page, D.C., Gerton, G.L., Davidson, I., and Wang, P.J. (2007). Abnormal sperm in mice lacking the Taf7l gene. *Mol. Cell Biol.* 27, 2582–2589. <https://doi.org/10.1128/MCB.01722-06>.
 46. Yoshida, K., Kondoh, G., Matsuda, Y., Habu, T., Nishimune, Y., and Morita, T. (1998). The mouse RecA-like gene Dmc1 is required for homologous chromosome synapsis during meiosis. *Mol. Cell.* 1, 707–718. [https://doi.org/10.1016/S1097-2765\(00\)80070-2](https://doi.org/10.1016/S1097-2765(00)80070-2).
 47. Martianov, I., Velt, A., Davidson, G., Choukallah, M.A., and Davidson, I. (2016). TRF2 is recruited to the pre-initiation complex as a testis-specific subunit of TFIIA/ALF to promote haploid cell gene expression. *Sci. Rep.* 6, 32069–32113. <https://doi.org/10.1038/srep32069>.
 48. Liu, S., Yu, H., Liu, Y., Liu, X., Zhang, Y., Bu, C., Yuan, S., Chen, Z., Xie, G., Li, W., et al. (2017). Chromodomain Protein CDYL Acts as a Crotonyl-CoA Hydratase to Regulate Histone Crotonylation and Spermatogenesis. *Mol. Cell.* 67, 853–866. <https://doi.org/10.1016/j.molcel.2017.07.011>.
 49. Xia, X., Zhou, X., Quan, Y., Hu, Y., Xing, F., Li, Z., Xu, B., Xu, C., and Zhang, A. (2019). Germline deletion of Cdy1 causes teratozoospermia and progressive infertility in male mice. *Cell Death Dis.* 10, 229. <https://doi.org/10.1038/s41419-019-1455-y>.
 50. Hogarth, C.A., Calanni, S., Jans, D.A., and Loveland, K.L. (2006). Importin α mRNAs have distinct expression profiles during spermatogenesis. *Dev. Dynam.* 235, 253–262. <https://doi.org/10.1002/dvdy.20569>.
 51. Kelley, J.B., Talley, A.M., Spencer, A., Gioeli, D., and Paschal, B.M. (2010). Karyopherin $\alpha 7$ (KPNA7), a divergent member of the importin α family of nuclear import receptors. *BMC Cell Biol.* 11, 63. <https://doi.org/10.1186/1471-2121-11-63>.
 52. Bolger, A.M., Lohse, M., and Usadel, B. (2014). Trimmomatic: a flexible trimmer for Illumina sequence data. *Bioinformatics* 30, 2114–2120. <https://doi.org/10.1093/bioinformatics/btu170>.
 53. Liao, Y., Smyth, G.K., and Shi, W. (2013). The Subread aligner: Fast, accurate and scalable read mapping by seed-and-vote. *Nucleic Acids Res.* 41, e108. <https://doi.org/10.1093/nar/gkt214>.
 54. Liao, Y., Smyth, G.K., and Shi, W. (2014). FeatureCounts: An efficient general purpose program for assigning sequence reads to genomic features. *Bioinformatics* 30, 923–930. <https://doi.org/10.1093/bioinformatics/btt656>.
 55. Robinson, M.D., McCarthy, D.J., and Smyth, G.K. (2010). edgeR: A Bioconductor package for differential expression analysis of digital gene expression data. *Bioinformatics* 26, 139–140. <https://doi.org/10.1093/bioinformatics/btp616>.
 56. Love, M.I., Huber, W., and Anders, S. (2014). Moderated estimation of fold change and dispersion for RNA-seq data with DESeq2. *Genome Biol.* 15, 550. <https://doi.org/10.1186/s13059-014-0550-8>.
 57. Huang, D.W., Sherman, B.T., and Lempicki, R.A. (2009). Systematic and integrative analysis of large gene lists using DAVID bioinformatics resources. *Nat. Protoc.* 4, 44–57. <https://doi.org/10.1038/NPROT.2008.211>.
 58. Pérez-Cerezales, S., Laguna-Barraza, R., De Castro, A.C., Sánchez-Calabuig, M.J., Cano-Oliva, E., De Castro-Pita, F.J., Montoro-Buils, L., Pericuesta, E., Fernández-González, R., and Gutiérrez-Adán, A. (2018). Sperm selection by thermotaxis improves ICSI

- outcome in mice. *Sci. Rep.* 8, 2902. <https://doi.org/10.1038/s41598-018-21335-8>.
59. Pérez-Cerezales, S., Miranda, A., and Gutiérrez-Adán, A. (2012). Comparison of four methods to evaluate sperm DNA integrity between mouse caput and cauda epididymidis. *Asian J. Androl.* 14, 335–337. <https://doi.org/10.1038/aja.2011.119>.
 60. Moreira, P.N., Jimenez, A., Fernández, R., Bury-Madrid, N., De La Fuente, J., Pintado, B., and Gutiérrez-Adán, A. (2003). Mouse ICSI with frozen–thawed sperm: The impact of sperm freezing procedure and sperm donor strain. *Mol. Reprod. Dev.* 66, 98–103. <https://doi.org/10.1002/MRD.10335>.
 61. Ramos-Ibeas, P., Calle, A., Fernández-González, R., Laguna-Barraza, R., Pericuesta, E., Calero, A., Ramírez, M.Á., and Gutiérrez-Adán, A. (2014). Intracytoplasmic Sperm Injection Using DNA-Fragmented Sperm in Mice Negatively Affects Embryo-Derived Embryonic Stem Cells, Reduces the Fertility of Male Offspring and Induces Heritable Changes in Epialleles. *PLoS One* 9, e95625. <https://doi.org/10.1371/JOURNAL.PONE.0095625>.
 62. Moreira, P.N., Fernández-González, R., Rizos, D., Ramirez, M., Perez-Crespo, M., and Gutiérrez-Adán, A. (2005). Inadvertent transgenesis by conventional ICSI in mice. *Hum. Reprod.* 20, 3313–3317. <https://doi.org/10.1093/HUMREP/DEI237>.
 63. Hourcade, J.D., Pérez-Crespo, M., Fernández-González, R., Pintado, B., and Gutiérrez-Adán, A. (2010). Selection against spermatozoa with fragmented DNA after postovulatory mating depends on the type of damage. *Reprod. Biol. Endocrinol.* 8, 9. <https://doi.org/10.1186/1477-7827-8-9>.
 64. Horiuchi, K., Perez-Cerezales, S., Papasaikas, P., Ramos-Ibeas, P., López-Cardona, A.P., Laguna-Barraza, R., Fonseca Balvis, N., Pericuesta, E., Fernández-González, R., Planells, B., et al. (2018). Impaired Spermatogenesis, Muscle, and Erythrocyte Function in U12 Intron Splicing-Defective Zrsr1 Mutant Mice. *Cell Rep.* 23, 143–155. <https://doi.org/10.1016/j.celrep.2018.03.028>.
 65. McCarthy, D.J., Chen, Y., and Smyth, G.K. (2012). Differential expression analysis of multifactor RNA-Seq experiments with respect to biological variation. *Nucleic Acids Res.* 40, 4288–4297. <https://doi.org/10.1093/nar/gks042>.
 66. Navarrete-López, P., Lombó, M., Maroto, M., Pericuesta, E., Fernández-González, R., Ramos-Ibeas, P., Parra, M.T., Viera, A., Suja, J.Á., and Gutiérrez-Adán, A. (2023). An ancient testis-specific IQ motif-containing H gene regulates specific transcript isoform expression during spermatogenesis. *Development* 150, 150. <https://doi.org/10.1242/dev.201334>.
 67. Uhlén, M., Fagerberg, L., Hallström, B.M., Lindskog, C., Oksvold, P., Mardinoglu, A., Sivertsson, Å., Kampf, C., Sjöstedt, E., Asplund, A., et al. (2015). Tissue-based map of the human proteome. *Science* 80, 347. <https://doi.org/10.1126/science.1260419>.
 68. Han, X., Wang, R., Zhou, Y., Fei, L., Sun, H., Lai, S., Saadatpour, A., Zhou, Z., Chen, H., Ye, F., et al. (2018). Mapping the Mouse Cell Atlas by Microwell-Seq. *Cell* 172, 1091–1107.e17. <https://doi.org/10.1016/j.cell.2018.02.001>.
 69. Macosko, E.Z., Basu, A., Satija, R., Nemesh, J., Shekhar, K., Goldman, M., Tirosh, I., Bialas, A.R., Kamitaki, N., Martersteck, E.M., et al. (2015). Highly parallel genome-wide expression profiling of individual cells using nanoliter droplets. *Cell* 161, 1202–1214. <https://doi.org/10.1016/j.cell.2015.05.002>.

STAR★METHODS

KEY RESOURCES TABLE

REAGENT or RESOURCE	SOURCE	IDENTIFIER
Antibodies		
Goat polyclonal anti-KPNA2 antibody	Invitrogen	PA1-32094; RRID: AB_2133674
Mouse monoclonal anti-goat IgG-HRP	Santa Cruz Biotechnology	SC-2354; RRID: AB_628490
Monoclonal anti- β -actin peroxidase-conjugated mouse antibody	Sigma-Aldrich	A3854; RRID: AB_262011
Donkey anti-mouse IgG-FICT	Santa Cruz Biotechnology	SC-2099; RRID: AB_641167
Rabbit polyclonal anti-ZNF384	Invitrogen	PA5-120411; RRID: AB_2913983
Rabbit polyclonal anti-TBPL1	Sigma-Aldrich	AV35751; RRID: AB_1858266
Rabbit polyclonal anti-PRDM9	FabGennix	PRDM9-901AP
Rabbit polyclonal anti-TAF7L	Invitrogen	PA5-100758; RRID: AB_2850261
Goat anti-rabbit	Invitrogen	A21245; RRID: AB_141775
Rabbit polyclonal anti-U2AF1L3/35	Santa Cruz	SC-368532
Goat monoclonal anti-mouse IgGk-HRP	Santa Cruz	SC-516102; RRID: AB_2687626
Critical commercial assays		
mMESSAGE mMACHINE T7 Ultra Kit	Thermo Fisher Scientific	AM1345
GeneArt™ Precision gRNA Synthesis Kit	Thermo Fisher Scientific	A29377
SURVEYOR® Mutation Detection Kit	Transgenomic	706020
Spermac® Kit	Minitube	15405/0000
Pierce™ BCA Protein Assay Kit	Thermo Fisher Scientific	23225
TUNEL <i>in situ</i> Cell Death Detection Kit	Roche	11684795910
Qubit® RNA Assay Kit	Life Technologies	Q32852
TruSeq RNA kit	Illumina	RS-122-2001
Deposited data		
Mouse reference genome, release 103, version GRCm39	Ensembl	http://ftp.ensembl.org/pub/release-103/fasta/mus_musculus/dna/
Mouse reference annotation, release 103, version GRCm39	Ensembl	http://ftp.ensembl.org/pub/release-103/gtf/mus_musculus
RNA-seq data from wild-type and <i>Kpna2</i> ^{-/-} testes	This paper	GEO: GSE213442
ChIP-Atlas	(Oki et al., 2018) ³⁵	https://chip-atlas.org/
Experimental models: Organisms/strains		
Mouse: B6CBAF1 (C57BL/6xCBA)	This paper	N/A
Oligonucleotides		
Primers for <i>Kpna2</i> ^{-/-} and WT genotyping, see Table S1	This paper	N/A
Primers for <i>Kpna2</i> ^{-/-} gRNA, see Table S1	This paper	N/A
Primers for <i>Kpna2</i> gene expression, see Table S1	This paper	N/A
Software and algorithms		
Integrated Semen Analysis System	Proiser	https://proiser.com/es/
SigmaStat	Systat	https://systatsoftware.com/
SPSS 16.0	IBM	https://www.ibm.com/es-es/spss

(Continued on next page)

Continued

REAGENT or RESOURCE	SOURCE	IDENTIFIER
FastQC v0.11.7	https://www.bioinformatics.babraham.ac.uk/projects/fastqc/	https://www.bioinformatics.babraham.ac.uk/projects/fastqc/
Trimmomatic v0.38	(Bolger et al., 2014) ⁵²	http://www.usadellab.org/cms/?page=trimmomatic
Subread v2.0.0	(Liao et al., 2013) ⁵³	https://subread.sourceforge.net/
featureCounts	(Liao et al., 2014) ⁵⁴	https://subread.sourceforge.net/
edgeR	(Robinson et al., 2010) ⁵⁵	https://bioconductor.org/packages/release/bioc/html/edgeR.html
DESeq2	(Love et al., 2014) ⁵⁶	https://bioconductor.org/packages/release/bioc/html/DESeq2.html
DAVID Functional Classification Tool	(Huang et al., 2009) ⁵⁷	https://david.ncifcrf.gov/
Cluster Locator	(Pazos Obregón et al., 2018) ²⁷	http://clusterlocator.bnd.edu.uy/
ChIP-Atlas	(Oki et al., 2018) ³⁵	https://chip-atlas.org/

RESOURCE AVAILABILITY

Lead contact

Further information and requests for resources should be directed to and will be fulfilled by the lead contact, Alfonso Gutiérrez-Adán (agutierr@inia.csic.es).

Materials availability

Mouse lines generated in this study are available from the [lead contact](#) upon request with a completed Materials Transfer Agreement.

Data and code availability

- RNA-seq data have been deposited at GEO and are publicly available as of the date of publication.
- The accession number for the raw and processed data files is GEO: GSE213442.
- Any additional information required to reanalyze the data reported in this paper is available from the [lead contact](#) upon request.

EXPERIMENTAL MODEL AND SUBJECT DETAILS

***Kpna2*-KO mice**

Cas9 and sgRNAs targeting the mouse *Kpna2* gene (Table S1) were produced using the mMACHINE mMESSAGE mACHINE T7 Ultra Kit and GeneArt™ Precision gRNA Synthesis Kit (Thermo Fisher Scientific, USA), respectively. The resultant RNAs were injected into B6CBAF1 (C57BL/6xCBA) zygotes, which were transferred to pseudo-pregnant CD1 females (Envigo, Madrid, Spain). Pups were genotyped by PCR conducted in standard conditions using *Kpna2* primers (Table S1) and screened for mutations using the SURVEYOR® Mutation Detection Kit (Transgenomic, NE, USA). Founders were confirmed by Sanger sequencing. Two transgenic lines with nonsense deletions that modify the amino acid sequence of the protein were successfully generated. Homozygous were used in all experiments. Wild-type (WT) and *Kpna2*^{+/-} (heterozygous) were used as controls. Animal experiments were conducted according to European legislation. All study protocols were approved by the Ethics Committee on Animal Experimentation of the INIA (Madrid, Spain) and were registered at the Dirección General de Agricultura y Ganadería de la Comunidad de Madrid (Spain) (PROEX 137.2/21). Throughout the manuscript, we use *Kpna2*^{-/-} to refer to results that are similar between the two selected lines, always carrying the mutation in homozygosity.

METHOD DETAILS

Sperm collection

Wild-type and *Kpna2*^{-/-} males were euthanized by cervical dislocation. Spermatozoa were collected by squeezing the vas deferens and dissecting the cauda epididymis. Spermatozoa were allowed to swim-out for 30 min at 37°C in a droplet of 500 µL HTF medium (2.04 mM CaCl₂, 101.6 mM NaCl, 4.69 mM

KCl, 0.37 mM KH_2PO_4 , 0.2 mM MgSO_4 , 21.4 mM sodium lactate, 0.33 mM sodium pyruvate, 2.78 mM glucose, 25 mM NaHCO_3 , 100 U/mL penicillin, 50 $\mu\text{g}/\text{mL}$ streptomycin and 0.001% (w/v) phenol red, supplemented with 1% (w/v) BSA). The concentration of the sperm sample was determined in a Thoma cell counting chamber. Sperm viability was assessed by eosin/nigrosin staining, examining 200 cells per male.⁵⁸

Sperm morphology

To assess sperm morphology, 6 μL of sperm suspension were spread on a slide and stained using the Spermac® Kit (Minitube) following the manufacturer's indications. The head of the sperm cell appears red, the acrosome, central piece, and tail green, and the equatorial zone is pale green, allowing for the identification of different abnormalities. These were classified into the categories: normal morphology, neck and midpiece defects, head defects and tail defects. The slides were observed under a light microscope (Nikon Eclipse E400), analyzing at least 200 cells per male from WT ($n = 6$) and $Kpna2^{-/-}$ males ($n = 6$).

Sperm motility analysis

6 μL of sperm suspension were placed in a Mackler® chamber on the stage of a microscope heated to 37°C (Nikon Eclipse E400) and fitted with a digital camera (Basler acA1300-200uc). Five 1.5-s videos were recorded and analyzed using the Integrated Semen Analysis System (ISAS® 2008). The parameters analyzed were as described by Pérez-Cereales et al.⁵⁸: straight-line velocity (VSL) (time-averaged velocity of the sperm head along a straight line from its first position to its last position, expressed in $\mu\text{m}/\text{s}$); curvilinear velocity (VCL) (time-averaged velocity of the sperm head along its actual curvilinear path, expressed in $\mu\text{m}/\text{s}$); average path velocity (VAP) (velocity over an average path generated by a roaming average between frames, expressed in $\mu\text{m}/\text{s}$); linearity (LIN) (defined as $(\text{VSL}/\text{VCL}) \times 100$); straightness (STR) (defined as $(\text{VSL}/\text{VAP}) \times 100$); wobble (WOB) (defined as $(\text{VAP}/\text{VCL}) \times 100$); amplitude of lateral head displacement (ALH) (width of the lateral movement of the sperm head, expressed in μm) and beatcross frequency (BCF) (number of times the sperm head crosses the direction of movement per second, expressed in Hz).

Gonadosomatic index

The testicles (6 from WT and 6 from KO mice) were extracted from each individual and weighed to establish the relationship between gonad and body size, a measure known as the gonadosomatic index (GSI).

Intracytoplasmic sperm injection (ICSI) and in vitro fertilization (IVF)

For our ICSI experiments, sperm were collected from the cauda epididymis and vas deferens in M2 medium (4 adult individuals) as described previously.⁵⁹ Sperm heads were decapitated by the freezing-thawing method.⁶⁰ The sperm sample was mixed with five volumes of a 10% solution of polyvinyl-pyrrolidone in M2. ICSI was performed in M2 medium at room temperature.⁶¹ In parallel, oocytes were collected at metaphase II from 8-week-old B6D2F1 females, which had been superovulated by standard intraperitoneal injection,⁶² and incubated with hyaluronidase (300 $\mu\text{g}/\text{mL}$) to remove cumulus cells.⁶³ After their recovery for 15 min, sperm was injected into the oocytes at M2 at room temperature (approximately 100 oocytes per replicate). Surviving zygotes were cultured until the blastocyst stage to check their development or until the 2-cell stage for embryo transfer experiments.

Western blots

Samples from the testicles of WT and $Kpna2^{-/-}$ mice were lysed in 300 μL of RIPA buffer containing 50 mM trisHCl pH 7.6, 150 mM NaCl, 1% Triton X-100, 0.5% sodium deoxycholate, and 0.1% SDS supplemented with COmplete™, EDTA-free Protease Inhibitor Cocktail (Roche) in constant agitation for 2 h at 4°C. The lysate was centrifuged at 12,000xg for 15 min, and the supernatant collected for protein analysis. Total protein was quantified using the Pierce™ BCA Protein Assay Kit (ThermoFisher Scientific) following the manufacturer's instructions. Proteins were separated on an SDS-PAGE gel (8% acrylamide, loading 50 μg of total protein per well) and transferred to a nitrocellulose membrane for immunoblotting following standard procedures. Blocking was conducted with 3% BSA in PBS-T (0.05% Tween) and membranes were incubated overnight at 4°C with a goat polyclonal anti-KPNA2 antibody (PA1-32094; Invitrogen) diluted 1:1000 in blocking solution. Incubation with the secondary antibody, mouse monoclonal anti-goat IgG-HRP (SC-2354; Santa Cruz Biotechnology) diluted 1:5000 in 1% BSA in PBS-T, took place for 2 h at room temperature. As a control, we used the monoclonal anti- β -actin peroxidase-conjugated mouse antibody

(A3854, Sigma-Aldrich). The chemiluminescence signal was digitalized using an ImageQuant LAS 500 chemiluminescence CCD camera (GE Healthcare Life Sciences, USA, 29005063).

Before western blotting of TAF7L and PRDM9, proteins were extracted from the testicles of WT and *Kpna2*^{-/-} mice and separated in the nuclear and cytoplasmic fractions with the Protein Fractionation Kit for Tissues (87790 ThermoFisher Scientific). For each tissue sample, to obtain cytoplasmic (C) fraction, cytoplasmic and membrane proteins were mixed and for nuclear (N) fraction, soluble nuclear and chromatin-bound proteins were mixed. Proteins were separated on an SDS-PAGE gel (8% acrylamide, loading 25 µg of total protein per well), transferred to a nitrocellulose membrane for immunoblotting following standard procedures. Blocking was conducted as described before with the following antibodies: a rabbit polyclonal anti-TAF7L antibody (PA5-100758, Invitrogen) diluted 1:1000 in blocking solution, a rabbit polyclonal anti-PRDM9 antibody (PRDM9-901-AP, Fabgennix International) diluted 1:500 in blocking solution, a rabbit polyclonal anti-U2AF1L3/35 (sc-368532, SantaCruz) diluted 1:1000 in blocking solution, and a mouse monoclonal anti-Adaptin-γ (AP-2) (610386, BD Transduction Laboratories) diluted 1:2000 in blocking solution. PRDM9, TAF7L and U2AF1/U2AF35 membranes were incubated with the secondary antibody, mouse monoclonal anti-goat IgG-HRP (SC-2354; Santa Cruz Biotechnology) diluted 1:5000 in 1% BSA in PBS-T, took place for 2 h at room temperature. AP-2 membrane was incubated with the secondary antibody, goat monoclonal anti-mouse IgGk-HRP (sc-516102, Santa Cruz) following the same procedure as the other membranes. The chemiluminescence HRP substrate used was Immobilon Forte Western HRP Substrate (Millipore). The chemiluminescence signal was digitalized as described before. Protein quantifications from membrane blotting were performed by Image J using Integrated density values.

Immunohistochemistry

Experimental and control testicles were examined through standard histological procedures. Briefly, testicles were fixed in 4% (w/v) paraformaldehyde and paraffin-embedded. Sections 4-µm sections from WT and *Kpna2*^{-/-} males were de-waxed, rehydrated and stained with hematoxylin and eosin.

To detect KPNA2, the sections were incubated in a buffer containing 10 mM sodium citrate and 0.05% Tween at 100°C for 20 min. After washing with distilled water, they were permeabilized in 1% PBS-T (triton X-100) for 20 min. Slides were then blocked in PBS supplemented with 3% BSA and 0.1% Tween for 1 h in a humid box. Next, they were incubated overnight at 4°C with anti-KPNA2 antibody (PA1-32094; Invitrogen) diluted 1:200 in blocking solution. Following three washing steps in PBS, the slides were incubated with the donkey anti-mouse IgG-FICT 1:300 (Santa Cruz Biotechnology; SC-2099) secondary antibody at 37°C for 1 h followed by washing three times in PBS and staining of the nuclei with 6.5 µg/mL Hoechst. VECTASHIELD Mounting Media for Fluorescence (Vector Laboratories, Peterborough, UK) was used for observation under a Nikon Eclipse TE-2000 confocal microscope (Nikon Instruments, Melville, New York, USA). Afterwards, a similar procedure was performed to examine the localization of ZFP384, TBPL1, PRMD9 and TAF7L, with the following specifications. The antibodies used were, respectively: anti-ZNF384 (PA5-120411; Invitrogen), anti-TBPL1 (AV35751; Sigma-Aldrich), anti-PRDM9 (PRDM9-901AP; FabGennix) and anti-TAF7L (PA5-100758; Invitrogen), all of them diluted 1:100. Following the incubation with the goat anti-rabbit secondary antibody 1:500 (A21245; Invitrogen) and the washing steps, we performed the staining of the acrosome and the nuclei with 15 µg/mL FITC-PNA and 6.5 µg/mL Hoechst, respectively.

TUNEL-assay

To detect apoptotic cells, testes were fixed in 4% PFA (neutral buffered, Sigma-Aldrich, MI, USA) and sections (5-mm) stained using the TUNEL *in situ* Cell Death Detection Kit (Roche, Basel, Switzerland) following the protocol provided by the manufacturer.⁶⁴ Apoptosis was scored by counting TUNEL fluorescent cells in 20 random cross-sections of seminiferous tubules from 5 WT and 5 mutant mice and expressed as the number of apoptotic cells per seminiferous tubule.

RNA-seq analysis

Total RNA was extracted from 4 testes of *Kpna2*^{-/-} mice and 4 testes of WT mice using TRIzol® reagent (Invitrogen, CA, USA) and then treated with DNase (Promega, WI, USA) for 1 h. The purified total RNA was stored in nuclease-free water and then used for first-strand synthesis. RNA concentrations were measured using a Qubit® RNA Assay Kit in a Qubit® 2.0 fluorometer (Life Technologies, CA, USA). RNA-seq libraries were prepared from the testes described above using the TruSeq RNA kit from Illumina® (NEB, USA) according to the manufacturer's recommendations. The cDNA libraries were then used for

sequencing with an Illumina® HiSeq2500 sequencer, generating an average of 54 million 150 bp paired-end reads per sample.

The quality of the resulting paired-end FASTQ files was evaluated using the FastQC tool v0.11.7 (<https://www.bioinformatics.babraham.ac.uk/projects/fastqc/>) before filtering and trimming, which was performed by means of Trimmomatic v0.38.⁵² Next, reads were mapped against the GRCm39 Ensembl reference genome using the Subread aligner v 2.0.0.⁵³ Prior to the downstream analysis, the gene count matrix was obtained by the read quantification software featureCounts,⁵⁴ using as reference the gene transfer format (GTF) from Ensembl.

Differential gene expression and functional characterization

After preprocessing, the genes were filtered out considering a threshold of 10 counts in at least 2 samples of any of the groups to improve the power of detection. Next, the TMM method was used to normalize samples accounting for the library size and RNA composition between samples. The differential expression analysis was conducted by overlapping the genes with FDR<0.05 obtained by the edgeR v3.36.0 and DESeq2 v1.34.0 methods, to increase reliability.^{55,56,65} Using the DAVID tool,⁵⁷ genes differing significantly between *Kpna2*^{-/-} mice and WT mice were subjected to GO (biological process, molecular function and cellular composition) and KEGG overrepresentation analyses, using an FDR below 0.05. Then, adjacent gene clustering and chromosome uniformity were evaluated using Cluster Locator, with a max-gap of 10 and p value of 0.05. The set of differentially expressed genes was analyzed for transcription factor enrichment via the web tool ChIP-Atlas,³⁵ which uses chromatin immunoprecipitation sequencing experiments (ChIP-seq). We considered experiments of all cell types, a distance of 5000 bp upstream and downstream from the transcription start sites and an adjusted p value cutoff of 0.01.

Classification of genes according to their expression in the different testis cell types

To characterize the set of DEGs we classified them in the testis cell types in a similar way as previously we have indicated.⁶⁶ Briefly, we integrated data from diverse studies that analyzed the gene expression profiles throughout the process of spermatogenesis.⁶⁶ The selected studies used different approaches or a combination of these: exploit of the first spermatogenic wave, purification of the major spermatogenic cell types and/or single-cell RNA-seq. Moreover, we also used data from the databases The Human Protein Atlas v20.1⁶⁷ and the Mouse Cell Atlas v2.0.⁶⁸ In addition, we processed and analyzed the single-cell transcriptomic data emerging from the study of Green et al.³¹ using the same reference annotation as our RNA-seq analysis for a finer-tuned classification. The raw data, produced using Drop-seq technology, was downloaded from GEO database (series GSE112393) and the preprocessing was performed using Drop-seq tools v2.4.0 from the McCarroll laboratory.⁶⁹ Altogether, DEGs were categorized in spermatogonia, spermatocytes, spermatids, Sertoli cells, Leydig cells, other somatic cells (macrophages, endothelial, innate lymphoid, peritubular myoid cells and fibroblasts) and spermatozoa.

Structural pairwise alignment

We performed the structural pairwise alignment of KPNA2 towards the rest α -importins expressed in testis using FATCAT flexible alignment.¹⁷ The .pdb structure files were retrieved from Alpha Fold (AF), with the following identifiers: AF-P52293-F1 (KPNA2), AF-Q60960-F1 (KPNA1), AF-O35345-F1 (KPNA6), AF-035344-F1 (KPNA3) and AF-035343-F1 (KPNA4).

QUANTIFICATION AND STATISTICAL ANALYSIS

Significant differences between KO and wild-type derived embryos produced by ICSI were assessed using ANOVA (SigmaStat package), respectively. The rest of the data (mean \pm SEM) were analyzed by one-way analysis of variance (ANOVA) followed by Duncan's or Tukey multiple range test using SPSS 16.0 software for comparisons of means. Significance was set at $p < 0.05$.